Identification of quiescent FOXC2^{+} spermatogonial stem cells in adult mammals

Zhipeng Wang[1,3], Cheng Jin[1,3], Pengyu Li[1], Yiran Li[1], Jielin Tang[1], Zhixin Yu[1], Tao Jiao[1], Jinhuan Ou[1], Han Wang[1], Dingfeng Zou[1], Mengzhen Li[1], Xinyu Mang[1], Jun Liu[1], Yan Lu[1], Kai Li[1], Ning Zhang[2], Jia Yu[1], Shiying Miao[1], Linfang Wang[1] and Wei Song[1*]

[1] Department of Biochemistry and Molecular Biology, State Key Laboratory of Medical Molecular Biology, Institute of Basic Medical Sciences Chinese Academy of Medical Sciences, School of Basic Medicine Peking Union Medical College; Beijing, 100005, China.
[2] MRC Protein Phosphorylation and Ubiquitylation Unit, School of Life Sciences, University of Dundee; Dundee, DD1 5EH, UK.
[3] These authors contributed equally: Zhipeng Wang, Cheng Jin.
* Correspondence: Wei Song

Email: songwei@ibms.pumc.edu.cn

Competing Interest Statement: The authors declare that they have no competing interests.

Classification: BIOLOGICAL SCIENCES and Developmental Biology

Keywords: FOXC2; spermatogonial stem cells; quiescence

Abstract

In adult mammals, spermatogenesis embodies the complex developmental process from spermatogonial stem cells (SSCs) to spermatozoa. At the top of this developmental hierarchy lie a series of SSC subpopulations. Their individual identities as well as the relationships with each other, however, remain largely elusive. Using single-cell analysis and lineage tracing, we discovered both in mice and humans the quiescent adult SSC subpopulation marked specifically by forkhead box protein C2 (FOXC2). All spermatogenic progenies can be derived from FOXC2$^+$ SSCs and the ablation of FOXC2$^+$ SSCs led to the depletion of the undifferentiated spermatogonia pool. During germline regeneration, FOXC2$^+$ SSCs were activated and able to completely restore the process. Germ cell specific *Foxc2* knockout resulted in an accelerated exhaustion of SSCs and eventually led to male infertility. Furthermore, FOXC2 prompts the expressions of negative regulators of cell cycle thereby ensures the SSCs reside in quiescence. Thus, this work proposes that the quiescent FOXC2$^+$ SSCs are essential for maintaining the homeostasis and regeneration of spermatogenesis in adult mammals.

Introduction

Through spermatogenesis, spermatozoa are generated from spermatogenic cells that are originated from spermatogonial stem cells (SSCs). It is critical for this process to be continuous and successful that SSCs are maintained in a homeostatic balance between self-renewal and differentiation (S. Sharma et al., 2019). The SSCs, which belong to a subgroup of undifferentiated spermatogonia (uSPG), exhibit significant heterogeneity and dynamic characteristics. In recent years, great insights into SSC behaviors and regulations have been provided by a body of pioneer works, especially with recent advances in single-cell gene-expression profiling, highlighting great heterogeneity of SSC and focusing on characterizing the nature of SSC states. Within the population of uSPG, a number of genes relatively higher expressed in primitive subfractions have been identified and well investigated, i.e., *Gfra1*, *ID4*, *Ret*, *Eomes*, *Pax7*, *Nanos2*, *Shisa6*, *T*, *Pdx1*, *Lhx1*, *Egr2* and *Plvap* (Aloisio et al., 2014; Guo et al., 2004; Hara et al., 2014; Helsel et al., 2017; Jijiwa et al., 2008; La et al., 2018; Nakagawa et al., 2021; Oatley et al., 2007; Sada et al., 2009; M. Sharma et al., 2019; Tokue et al., 2017). Particularly, *Gfra1*, *ID4*, *Eomes*, *Pax7*, *Nanos2*, and *Plvap* are further validated through lineage tracing experiment, which is considered to be a reliable method to study the development of stem cells. However, some essential and primitive sub-populations remain undiscovered, and the identification of which is of great significance for elucidating the developmental process of SSC renewal and its behavior in testis.

Adult stem cells (ASCs), as the undifferentiated primitive cells that can be found in nearly all types of tissues in mammals, are characteristic for a unique quiescent status reflected by both reversible cell cycle arrest and specific metabolic alterations (van Velthoven & Rando, 2019). The role of the quiescent stem cells is to avoid premature exhaustion and to allow the long-term maintenance of a functional stem cell pool (Cheung & Rando, 2013). The adult SSCs appear to share this characteristic, as revealed in recent single-cell RNA-sequencing (scRNA-seq) analysis in humans and mice, being largely non-proliferative while capable of reciprocating between the quiescent and activated status during homeostasis and regeneration (Guo et al., 2018; Hermann et al., 2018; Suzuki et al., 2021; Tan & Wilkinson, 2019; Wang et al., 2018). This notion has also been significantly supported by the discoveries of important regulators such as USF1 (Faisal et al., 2019) and DNMT3L (Liao et al., 2014) as well as the pathways including the PI3K/MAPK and mTORC1 signalings (Suzuki et al., 2021). In addition, it is generally believed that cells in a quiescent state are supposed to be more resilient to genotoxic insults, thus theoretically the

quiescent SSCs can restore spermatogenesis upon such disturbance. However, by large, much remain unknown as to the characteristics and regulation of the quiescence state of adult SSCs. Thus, more important insights can be obtained through searching the quiescent SSC population and defining the essential characteristics of this population as the foundation of successful spermatogenesis.

Forkhead box protein C2 (FOXC2), a member of the forkhead/winged helix transcription factor family, plays essential roles in the development of various tissues in mice (Bahuau et al., 2002; Kume et al., 2001; Motojima et al., 2016; Sasman et al., 2012). Recently, FOXC2 has been found to be expressed in A_s and A_{pr} spermatogonia of mouse testes and is required for SSC maintenance (Wei et al., 2018). However, the role of FOXC2 in the development of adult SSCs *in vivo* has yet to be explored. In this study, we identified a subpopulation of adult SSCs specifically expressed by FOXC2. In adult mice, FOXC2$^+$ SSCs gave rise to all spermatogenic progenitor cells that can complete the full spermatogenesis. Upon the loss of FOXC2$^+$ SSCs, the undifferentiated spermatogonia pool was exhausted, eventually leading to defective spermatogenesis. Specifically, FOXC2 is required for maintaining SSC quiescence by promoting the expression of negative regulators of cell cycle. Moreover, the FOXC2$^+$ population endured the chemical insult with busulfan and effectively restored spermatogenesis. Overall, we propose that FOXC2$^+$ represents the quiescent state of the SSCs in adult mammals that is crucial for the homeostasis and regeneration of SSCs.

Results

Identification of FOXC2$^+$ SSCs from the adult uSPGs. We performed single-cell RNA-seq (10x genomics) of the uSPG from adult mice testes marked by THY1, a widely recognized surface marker for uSPG with self-renewing and transplantable state (Hammoud et al., 2014; Kubota et al., 2004), to dissect the heterogeneity and developmental trajectory (Figure 1A, Figure 1—figure supplement 1A, B). Among 5 distinct clusters identified, Cluster1 was characterized by the high expression of stemness markers whereas other clusters were featured by progenitor or differentiating spermatogonia (dSPG) markers (Figure1B, Figure 1—figure supplement 1C, D). Primarily mapped to the extreme early point of the developmental trajectory, Cluster1 cells appeared quiescent and likely represented the primitive state of uSPG populations (Figure1B, Figure 1—figure supplement 1E-G). The top10 differentially expressed genes (DEGs) associated with Cluster1 are featured by SSC markers such as *Mcam* (Kanatsu-Shinohara et al., 2012), *Gfra1* (Hara et al., 2014), *Tcl1* and *Egr2* (Hermann et al., 2018; La et al., 2018) (Figure1C, Figure 1—figure supplement 2A, Figure 1—source data 1) in addition to six others expressed in different stages of germ cells and/or somatic cells, in which only FOXC2 was exclusively localized in the nucleus of a subgroup of ZBTB16$^+$ uSPG in mice (Buaas et al., 2004; Costoya et al., 2004) (Figure 1D, Figure 1—figure supplement 2B). More specifically, FOXC2 displayed differential expressions among various subtypes of uSPG, being more specific in A_s (59.9%) than other subtypes including A_{pr} (5.2%), A_{pr-1} (4.1%), A_{al4-1} (1.83%), A_{al8-1} (1.5%), and A_{al16-1} (1.67%) (Figure 1E). There was only a small fraction (5.1%) was active in proliferation as indicated by MKI67 (Figure 1F), suggesting that FOXC2$^+$ cells are primarily quiescent. Additionally, when examining the SSC markers validated previously by lineage tracing (La & Hobbs, 2019), we found that FOXC2 displays a higher level of co-localization with GFRA1 and EOMES than PAX7 and NEUROG3 (Nakagawa et al., 2007), indicating the FOXC2$^+$ cells contain but differ from the known SSC subsets (Figure 1G).

We next analyzed the expression of FOXC2 in adult human testis using the published scRNA-seq dataset (GSE112013) (Guo et al., 2018). As expected, FOXC2 was also specifically expressed in the human SSCs, most of which were MKI67$^-$ (Figure 1H, Figure 1—figure supplement 2C). Pseudotime analysis showed that the FOXC2$^+$ cells located at the start of the developmental trajectory with a proportion of about 90% that were MKI67$^-$ (Figure 1I). Immunofluorescence staining confirmed that FOXC2$^+$ cells were a subset of ZBTB16$^+$ spermatogonia in adult human testis, and most of them were MKI67$^-$ (Figure 1J), representing a quiescent subpopulation of SSCs in human testis(Clermont, 1966a, 1966b, 1969; Ehmcke & Schlatt, 2006; Ehmcke et al., 2006). These results suggest that FOXC2 is similarly expressed in the SSCs of adult human and mouse testis and may possess a conserved function.

FOXC2$^+$ SSCs sufficiently initiate and sustain spermatogenesis. We generated *Foxc2$^{iCreERT2/+}$;Rosa26$^{LSL-T/G/LSL-T/G}$* mice in which FOXC2$^+$ cells were specifically labeled with GFP to enable the progeny tracing after tamoxifen treatment (Figure 2—figure supplement 1) (Wang et al., 2015). Tamoxifen was introduced at 2-month of age, after which the FOXC2-expressing lineage (GFP$^+$) was tracked at d3 (day3), w1 (week1), w2, w4, w6, m4 (month4), m7, and m12 respectively (Figure 2A). At d3, the tracked cells were both GFP$^+$ and FOXC2$^+$ (Figure 2B) and constituted 0.027% of the total testicular cells as indicated by the fluorescence-activated cell sorting (FACS) analysis (Figure 2C). GFP$^+$ cells and THY1$^+$ cells sorted by FACS were then transplanted into testes of recipient mice pre-treated with busulfan, respectively. Two months after transplantation, FOXC2$^+$ cells generated 3.6 times greater number of colonies than the THY1$^+$ control (Figure 2D,

132 E), indicating that the FOXC2$^+$ cells possess higher stemness as convinced by stronger
133 transplantable viability.
134 At w1, all GFP$^+$ cells were identified as uSPGs, encompassing A_s, A_{pr}, and $A_{al\text{-}4}$ (Figure 2F_a).
135 Specifically, FOXC2$^+$ A_s gave rise to 3 types of A_{pr}, i.e., FOXC2$^+$/FOXC2$^+$, FOXC2$^+$/FOXC2$^-$, and
136 FOXC2$^-$/FOXC2$^-$ (Figure 2$F_{c1, b, c2, d2}$), which then either produced FOXC2$^+$ or FOXC2$^-$ A_s through
137 symmetric or asymmetric division (Figure 2$F_{c3, d1, f1}$), or developed into A_{al} with no more than one
138 FOXC2$^+$ cell in the chains (Figure 2$F_{e, f2}$). These results confirm that FOXC2$^+$ cells are capable of
139 self-renewal to sustain the population as well as replenishing the uSPG pool by producing
140 downstream progenies, thereby serving as SSCs. In the following 2-6 weeks, GFP$^+$ colonies further
141 expanded and produced GFP$^+$ sperms in the epididymis, from which healthy GFP$^+$ offspring were
142 given birth by C57BL/6J female recipients (Figure 2G). The GFP$^+$ colonies constituted 83.67%,
143 90.48%, 96.78%, 98.55%, and 99.31% of the total length of the seminiferous tubules at w6, m2,
144 m4, m7, and m12 respectively (Figure 2H, I). All offspring were GFP$^+$ from m4 onwards (Figure 2J).
145 Additionally, the EOMES$^+$, GFRA1$^+$ and PAX7$^+$ cells were all GFP$^+$ at w2, further confirming these
146 progenies were derived from the FOXC2$^+$ cells (Figure 2K). Overall, FOXC2$^+$ SSCs can produce
147 all subtypes of uSPG, thus initiating spermatogenesis in adult mice.
148
149 **Specific ablation of the FOXC2$^+$ SSCs results in the depletion of uSPG pool.** We then prepared
150 *Foxc2$^{iCreERT2/+}$;Rosa26$^{LSL\text{-}DTA/+}$* mice to investigate the physiological requirement of FOXC2$^+$ SSCs
151 in spermatogenesis (Wang et al., 2015). FOXC2$^+$ population in 2-month-old mice was specifically
152 ablated with tamoxifen-induced diphtheria toxin (DTA). The testes of these mice were examined at
153 d3, d7, and d14 post tamoxifen induction (Figure 3A). Gradual loss of weight in testes coincided
154 with the reduction in the size of testes in all the mice while body weight was maintained (Figure 3B,
155 C). Specifically, at d3, there were no detectable FOXC2$^+$ cells in addition to the decrease in the
156 number of GFRA1$^+$, LIN28A$^+$ (Zheng et al., 2009) and ZBTB16$^+$ uSPG at the basement membrane
157 of seminiferous tubules; at d14, all GFRA1$^+$, LIN28A$^+$ and ZBTB16$^+$ uSPG disappeared while
158 vacuoles formed at the basement membrane with remaining spermatocytes and spermatids in the
159 seminiferous lumen (Figure 3D–F, Figure 3—figure supplement 1). Meanwhile, the expression of
160 DDX4 (Toyooka et al., 2000) and DAZL (Li et al., 2019) as germ cell markers was significantly
161 reduced along with nearly undetectable expression of uSPG markers such as ZBTB16, LIN28A,
162 GFRA1, RET, and NEUROG3 (Nakagawa et al., 2007) (Figure 3G). These results indicate an
163 uSPG exhaustion as the result of the FOXC2$^+$ SSCs ablation, therefore supporting the critical role
164 played by FOXC2$^+$ population in spermatogenesis.
165
166 **FOXC2$^+$ SSCs are resistant to busulfan and indispensable for germline regeneration.** Next,
167 we examined the regenerative viability of FOXC2$^+$ SSCs. At d20 post busulfan treatment
168 (20mg/kg), FOXC2$^+$ cells constituted the majority of uSPGs (Figure 4A). Following a sharp
169 decrease in cell number in the first five days, ZBTB16$^+$ and GFRA1$^+$ cells began to recover from
170 d25 while the number of FOXC2$^+$ cells remained stable (Figure 4B), indicating that this population
171 is insensitive to busulfan. We then checked changes in the proportion of MKI67$^+$ cells in FOXC2$^+$
172 population after busulfan treatment (Figure 4C, D). At d30, the MKI67$^+$ proportion rose to 15.92%,
173 indicating a higher level of proliferation, albeit the total cell number stayed static (Figure 4B, D),
174 thereby becoming the driving force in restoring spermatogenesis. Up to d120, the MKI67$^+$
175 proportion had settled gradually back to the pre-treatment level, accompanied by the full recovery
176 of spermatogenesis (Figure 4D). Further details of this process were revealed during lineage
177 tracing (Figure 4E). Three days after tamoxifen induction, the 2-month-old
178 *Foxc2$^{iCreERT2/+}$;Rosa26$^{LSL\text{-}T/G/LSL\text{-}T/G}$* mice were treated with busulfan. Consistent with the results

179 above, at d20, the survived uSPGs were predominantly GFP$^+$ (Figure 4F). Over 68.5% of the total
180 length of the seminiferous tubules were GFP$^+$ at m2, and this proportion rose to 95.43%, 98.41%,
181 and 99.27% at m4, m7, and m12 respectively (Figure 4G, H), which was comparable to the
182 proportion by tamoxifen induction alone (Figure 2I). From m4 onwards, nearly all germ cells,
183 spermatids, and their offspring were GFP$^+$ (Figure 4G, I). Together, these results confirm that
184 FOXC2$^+$ SSCs are indispensable for germline regeneration that is central to spermatogenesis
185 recovery from interruptions.
186
187 **FOXC2 is essential for SSC maintenance in adult mice.** We then focused on dissecting the role
188 of FOXC2 in the SSC maintenance using *Foxc2$^{f/-}$;Ddx4$^{Cre/+}$* mice (Gallardo et al., 2007) (Figure 5A).
189 No significant difference was observed in the expressions of various uSPG markers, including
190 ZBTB16 and LIN28A, between *Foxc2$^{f/-}$;Ddx4$^{Cre/+}$* and *Foxc2$^{f/+}$* mice at the age of 1 week (Figure
191 5—figure supplement 1A). However, adult *Foxc2$^{f/-}$;Ddx4$^{Cre/+}$* mice displayed clear testis weight loss
192 without significant body weight loss (Figure 5B, C). Moreover, in these mice, we observed severe
193 degeneration of seminiferous tubules, reduced number of spermatids in the epididymis, and
194 decreased size of the uSPG population with age (Figure 5D–G) but without apparent signs of
195 apoptosis (Figure 5—figure supplement 1B). The 6-month-old *Foxc2$^{f/-}$;Ddx4$^{Cre/+}$* mice were infertile,
196 in which over 95% seminiferous tubules were Sertoli-only with hardly detectable expressions of
197 DAZL, DDX4, LIN28A, and ZBTB16 (Figure 5D–F, H). Therefore, FOXC2 is essential for
198 maintaining the SSC homeostasis and normal spermatogenesis in adult mice.
199
200 **FOXC2 maintains the quiescent state of SSCs through negatively regulating the cell cycle.**
201 We collected THY1$^+$ uSPGs from 4-month-old *Foxc2$^{f/+}$* and *Foxc2$^{f/-}$;Ddx4$^{Cre/+}$* mice and compared
202 their transcriptome signatures revealed from scRNA-seq (Figure 6A). The pseudotime analysis
203 identified Cluster1, which represented the FOXC2-expressing SSCs in *Foxc2$^{f/+}$* mice corresponding
204 to the FOXC2-deleting SSCs in the *Foxc2$^{f/-}$;Ddx4$^{Cre/+}$* mice, was specifically assigned to the
205 extremely early stage of the development trajectory in respective samples, which was validated by
206 the expression of corresponding markers (Figure 6B, Figure 6—figure supplement 1A, B).
207 Aggregated analysis of the overall uSPG populations showed that cells derived from
208 *Foxc2$^{f/-}$;Ddx4$^{Cre/+}$* mice were specifically associated with the late stage of the development
209 trajectory, as opposed to *Foxc2$^{f/+}$* mice where nearly all the cells derived were concentrated at the
210 early stage of development (Figure 6C, Figure 6—figure supplement 1C). This implies that the loss
211 of FOXC2 prompts the SSCs to progress into a more differentiated stage. Further analysis of the
212 cells in Cluster1 revealed two distinct subclusters, i.e., Subclusters0 and Subclusters1 (Figure 6—
213 figure supplement 2A). Formed primarily by the Cluster1 cells derived from *Foxc2$^{f/+}$* mice,
214 Subclusters0 was featured by stemness markers, while Subcluster1, representing the majority of
215 Cluster1 cells from *Foxc2$^{f/-}$;Ddx4$^{Cre/+}$* mice, was featured by progenitor markers (Figure 6—figure
216 supplement 2B, C). Consistently, pseudotime analysis showed that Cluster1 cells from *Foxc2$^{f/+}$*
217 mice projected a forward stage of the developmental trajectory indicated by stemness markers,
218 whereas Cluster1 cells from *Foxc2$^{f/-}$;Ddx4$^{Cre/+}$* mice were associated with a later stage of the
219 developmental trajectory (Figure6D, Figure 6—figure supplement 2D, E). More specifically, less
220 number of cells were found at the starting state1 in Cluster1 from *Foxc2$^{f/-}$;Ddx4$^{Cre/+}$* mice than in
221 *Foxc2$^{f/+}$* mice, with rather more cells in the developmental progression (from state1 to state5),
222 especially at the advanced state5 (Figure 6E). Thus, FOXC2 deletion caused defective SSC
223 maintenance and committed the SSCs to a differentiation destiny. Further, there were 932 genes
224 down-regulated in Cluster1 cells derived from *Foxc2$^{f/-}$;Ddx4$^{Cre/+}$* mice in comparison to *Foxc2$^{f/+}$* mice
225 (Figure 6F, Figure 6—source data 1), which were functionally associated with both stem cell

population maintenance and mitotic cell cycle (Figure 6G). Consistently, the GSEA analysis revealed a more progressive cell cycle in Cluster1 upon *Foxc2*-knockout (Figure 6H), confirming the role of FOXC2 in regulating the cell cycle of the SSCs.

We then performed Cleavage Under Targets and Tagmentation (CUT&Tag) sequencing to explore the underlying mechanism (Kaya-Okur et al., 2020; Kaya-Okur et al., 2019), for which GFP$^+$ SSCs from *Foxc2*$^{iCreERT2/+}$;*Rosa26*$^{LSL\text{-}T/G/LSL\text{-}T/G}$ mice 3 days after tamoxifen induction, representing the FOXC2$^+$ SSCs, were isolated for CUT&Tag sequencing (Figure 7A). Specific peaks enriched in the promoter region of 3629 genes (Figure 7B, C; Figure 7—source data 1) showed functional enrichment in biological processes such as DNA repair and mitotic cell cycle regulation (Figure 7D). By overlapping with the 932 genes down-regulated in Cluster1 cells from *Foxc2*$^{f/-}$;*Ddx4*$^{Cre/+}$ mice, we obtained 306 genes as the candidates subjective to the regulation by FOXC2 (Figure 7E; Figure 7—source data 1). Further, Gene Ontology (GO) enrichment analysis of these genes highlighted a distinctive functional cluster (11 genes) focusing on the negative regulation of cell cycle (Figure 7F; Figure 7—source data 1) (Bahar et al., 2002; Bakker et al., 2004; Gaudet et al., 2011; Georgescu et al., 2014; Knudson & Korsmeyer, 1997; Nitiss, 2009; Raman et al., 2007; van Oosten et al., 2005; Weaver et al., 2003; Yi et al., 2012). More specifically, significant peaks enrichment at the promoter region were observed for these candidate genes (Figure 7G). Meanwhile, as predicted using the JASPAR Scan function (binding potential >0.8), there showed strong binding potential of FOXC2 towards these candidate genes (Figure 7I) via the binding motif of FOXC2 (Figure 7H), which was further confirmed by the result from the CUT&Tag qPCR (Figure 7J). Overall results imply that FOXC2 may function as a gatekeeper that ensures the quiescent state of SSCs by impeding cell cycle progression.

Discussion

In this work, a comprehensive analysis of uSPG populations with scRNA-seq and the following lineage tracing study by whole-mount immunofluorescence assay led to the identification of FOXC2$^+$ SSCs as a quiescent SSC subpopulation in adult mice. Further investigation through functionality analysis confirmed FOXC2 is essential for SSC self-renewal and stemness, thereby is required for maintaining the SSC population that is critical for continuous spermatogenesis. Importantly, our data demonstrated that the colonies formed by FOXC2$^+$ cells constituted nearly the total length of the seminiferous tubules (99.31%), implying that the FOXC2$^+$ SSCs can support the complete spermatogenesis in adult mice.

GFRA1$^+$ A_{pr} and A_{al} cells are found to break randomly and a portion of them can return to the stem cell state (Hara et al., 2014). Interestingly, our findings showed FOXC2 appeared in one of the A_{pr} or A_{al} cells at times, therefore raising a possibility that the subset of GFRA1$^+$ cells that return to stem cell state after intercellular bridge break, maybe FOXC2$^+$ due to different cell cycle state. If so, based on both findings, GFRA1$^+$FOXC2$^+$ could represent a quiescent state whereas GFRA1$^+$FOXC2$^-$ is proliferate active, which certainly requires further validation possibly through multiple lineage tracing and live imaging.

We observed that the FOXC2$^+$ SSCs were almost all in a non-proliferative state (~94.9%), and further revealed that FOXC2 functioned in the negative regulation of cell cycle progression, thus confirming that FOXC2-expressing SSCs are quiescent SSC population in adult mice. The finding that FOXC2 inhibited cell cycle and differentiation of SSCs in testis is consistent with that reported in other tissues (Davis et al., 2004; Sabine et al., 2015). In general, the quiescent state is a protective mechanism for stem cell storage and prevents stem cells from damage or depletion under genotoxic stresses (Arai & Suda, 2007; Relaix & Zammit, 2012; Rodgers et al., 2014; S.

Sharma et al., 2019). In our work, after the busulfan treatment, the quantity of FOXC2$^+$ cells remained stable and the survived uSPGs were predominantly FOXC2$^+$, indicating its insensitivity to cytotoxic agents. However, the proportion of MKI67$^+$FOXC2$^+$ cells increased by 15.92% after 30 days of the busulfan treatment and decreased back to the pre-treatment level (5.08%) at 120 days, implying that the quiescent FOXC2$^+$ cells are able to transform into the proliferative FOXC2$^+$ cells to replenish the SSC pool to maintain the SSC homeostasis and normal spermatogenesis. We further confirmed by lineage tracing analysis that FOXC2-expressing cells were the only remaining SSC population and were responsible for germline regeneration after the busulfan treatment, indicating that FOXC2$^+$ SSCs represent a functionally important stem cell population with regenerative ability. In the future, more insights into the unique regulation of SSCs can be drawn from studying and comparing the transition between the quiescent and proliferative states in FOXC2$^+$ and other SSC subpopulations.

According to our findings, we propose a model for the maintenance of the FOXC2$^+$ SSC subpopulation (Figure 7K). Under physiological conditions, FOXC2$^+$ A_s cells (including FOXC2$^+$GFRA1$^+$, FOXC2$^+$EOMES$^+$ cells, etc.) constitute the SSC pool, of which only a small proportion (~5.1%) cells are proliferative while the majority remains quiescent (Figure 7Ka). This population can divide symmetrically or asymmetrically into different A_{pr} and A_{al} (Figure 7Kb). Then FOXC2$^+$ cells (Figure 7Kb) may break from the syncytial and return to A_s state (Figure 7Ka) to maintain the stable number of the SSC pool. FOXC2$^-$ progenies, derived from the FOXC2$^+$ population, form progenitors (Figure 7Kc) to support spermatogenesis. However, it requires continuous supply from the FOXC2$^+$ population and is subject to exhaustion when the supply is disrupted. In the context of regeneration conditions, the FOXC2$^+$MKI67$^-$ cells can survive and set out the recovery process (Figure 7Kd). At the early stage, increasing proportion of FOXC2$^+$MKI67$^-$ cells is committed to transforming into proliferative FOXC2$^+$MKI67$^+$ cells, strengthening the supply to the progenitors (Figure 7Ke). At the late recovery stage, MKI67$^+$/MKI67$^-$ ratio returns to the physiological level in FOXC2$^+$ population (Figure 7Ka), leaving the total number of FOXC2$^+$ cells stable, therefore maintaining the SSC homeostasis. However, it is necessary to perform more investigation to further improve and modify this model to gain a complete understanding of the connections between different SSC subpopulations in the testes of adult mice.

Based on our observation, FOXC2 seems nonessential for the transformation from gonocytes to SSCs in infant mice, in contrast to its requirement for adult spermatogenesis. A recent study showed that FOXC2$^+$ subpopulation in the postnatal mouse testis (<5 weeks) appeared more active in proliferation than the adult counterpart (Wei et al., 2018). Such differential functionality might reflect the difference in the physical nature of spermatogenesis between developmental stages. For example, the maturity of spermatogenesis is still under development during the juvenile period with a focus on establishing and expanding the SSC pool. Therefore, it would be interesting to explore differences in individual functional contexts as well as the underlying regulatory mechanisms. Meanwhile, FOXC2, highly conserved between mice and humans with 94% identity in amino acid sequence (Miura et al., 1997), is also expressed in a subset of human adult SSCs, raising the possibility of an evolutionarily conserved mechanism governing SSC homeostasis in humans. Further work following this direction might be of great clinical significance specifically to patients who suffer from infertility. Moreover, the developmental correlation between FOXC2$^+$ SSCs and other SSC subpopulations proposed previously should be revealed via biological methods such as multiple lineage tracing and live imaging. Collectively, our work here provides new insights into the investigation of adult SSCs and serves as a reference for studying the homeostasis and regeneration of other stem-cell systems.

Materials and methods

Mice

Animal experiments were approved by the Committee on Animal Care of the Institute of Basic Medical Sciences, Chinese Academy of Medical Sciences and Peking Union Medical College. The tab of animal experimental ethical inspection (No: ACUC-A01-2018-017) has been provided in supplementary file. The 8-week-old C57BL/6J wild-type mice were used for magnetic-activated cell sorting. The *Rosa26*$^{LSL\text{-}T/G/LSL\text{-}T/G}$ mice (stock no. 007676), *Ddx4*$^{Cre/+}$ mice (stock no. 000692) and EGFP$^{Tg/+}$ mice (stock no. 021930) were bought from the Jackson Laboratory. The *Foxc2*^{iCreERt2} mice and the *Foxc2*$^{flox/flox}$ (*Foxc2*$^{f/f}$) mice were constructed and bought from the Biocytogen. The *Rosa26*$^{LSL\text{-}DTA/+}$ mice were bought from GemPharmatech. All mice were housed and bred under specific pathogen-free conditions (temperature: 22-26°C, humidity: 40-55%, 12-h light/dark cycle) in the animal facility at the Institute of Basic Medical Sciences. DNA was isolated from the tails, and the genotypes of the mice were checked using PCR with specific primers (Materials and methods—source data 1). All mice were randomly assigned to experiments and no statistical methods were used to predetermine sample size. The person performing the experiments did not know the sample identity until after data analysis. No data were excluded from analyses and the data displayed included a minimum of three independent experiments and a minimum of three biological replicates for each independent experiment. The 8-week-old C57BL/6J WT mice were treated with busulfan (40 mg/kg) and used as recipient mice 1 month later.

Magnetic-activated cell sorting (MACS)

The testes from 8-week-old C57BL/6J wild-type mice or 4-month-old *Foxc2*$^{f/+}$ and *Foxc2*$^{f/-}$;*Ddx4*$^{Cre/+}$ mice (n=4) were minced and digested in the collagenase type IV (1 mg/mL, Sigma) and DNase I (500μg/mL, Sigma) at 37°C for 15 min. The cell suspension was pipetted up and down once every 5 minutes and the digestion process was stopped with DMEM (containing 10% FBS). The cell suspension was filtered through a 40-μm nylon mesh, and after centrifugation, the cells were resuspended in 8 mL PBS. The 15 mL conical centrifuge tubes were slowly overlayed with 2 mL of 70% Percoll solution, 2 mL of 30% Percoll solution, and then 2 mL of testicular cell suspension and centrifuge at 600 × g for 10 min at 4 °C without using the centrifuge brake. After centrifugation, the cells at the interface between the 70% and the 30% Percoll solution were carefully removed into the new conical centrifuge tubes, washed with PBS, and then centrifuge at 600 × g for 10 min at 4 °C. After centrifugation, the cells were resuspended in 360μL MACS buffer, added with 40μL of magnetic microbeads conjugated with anti-Thy-1 antibody (Miltenyi Biotec 130–049–101, Auburn, CA), and mixed well. Incubate the cell suspension containing Thy-1 microbeads for 20 min at 4 °C. Mix gently by tapping every 10 min. Add 20 mL of MACS buffer to the tube to dilute Thy-1 microbeads and centrifuge at 300 ×g for 10 min at 4 °C. Remove the supernatant completely and resuspend in 2 mL of MACS buffer. Place the separation columns (MS Column; Miltenyi Biotec 130-042-201) in the magnetic field of the mini MACS Separation Unit (Miltenyi Biotec 130-142-102) and rinse with 0.5 mL of MACS buffer. Apply the cell suspension to the columns (500μL/ column). After the cell suspension has passed through the column and the column reservoir is empty, wash the column with 0.5 mL of MACS buffer three times. Remove the column from the MACS Separation Unit and elute the magnetically retained cells slowly into a 50 mL conical centrifuge tube with 1 mL of MACS buffer using the plunger supplied with the column. Centrifuge the tube containing the cells at 600 × g for 10 min at 4 °C and resuspend the cell pellet with 10 mL of MACS buffer for rinsing. Repeat this step once. After the final rinsing step, resuspend cells in 0.04% BSA and count the cell number.

367
368 **Single-cell RNA-seq**
369 The MACS-sorted THY1^{+} cells were used for loading onto the Chromium Single Cell 3′ Chip kit v2
370 (10x Genomics, PN-120236) according to the instructions. Cell capturing and library preparation
371 was performed following the kit instructions of the Chromium Single Cell 3' v2 Library and Gel Bead
372 Kit (10x Genomics, PN-120237). In brief, 5000 cells were targeted for capture, and after cDNA
373 synthesis, 10-12 cycles were used for library amplification. The libraries were then size-selected,
374 pooled, and sequenced on a Novaseq 6000 (Illumina). Shallow sequencing was performed to
375 access the library quality and to adjust the subsequent sequencing depth based on the capture
376 rate and the detected unique molecular indices (UMI).
377
378 **Single-cell RNA-seq data processing**
379 Raw sequencing reads were processed using the Cell Ranger v.3.0.1 pipeline of the 10x Genomics
380 platform. In brief, reads from each sample were demultiplexed and aligned to the mouse mm10
381 genome, and UMI counts were quantified for each gene per cell to generate a gene-barcode matrix.
382 Default parameters were used. The UMI counts were analyzed using the Seurat R Package (Stuart
383 et al., 2019) (v.3.0.1) following the Seurat pipeline. Cells with more than 200 detected genes or less
384 than 10% mitochondria reads were retained. Genes not detected in at least 10 cells were removed
385 from subsequent analysis. The resulting matrix was normalized, and the most variable genes were
386 found using Seurat's default settings, then the matrix was scaled with regression against the
387 mitochondria reads. The top 2000 variable genes were used to perform PCA, and Jackstraw was
388 performed using Seurat's default settings. Variation in the cells was visualized by UMAP for the top
389 principal components. Cell types were determined using marker genes identified from the literature
390 (Kowalczyk et al., 2015). We used the Seurat function CellCycleScoring to determine the cell cycle
391 phase, as this program determines the relative expression of a large set of G2-M and S-phase
392 genes. After removing the undefined cells, the spermatogonia were used for trajectory analysis,
393 and the single-cell pseudotime trajectory was constructed with the Monocle 2 package (v2.12.0)
394 (Qiu, Hill, et al., 2017; Qiu, Mao, et al., 2017; Trapnell et al., 2014) according to the provided
395 documentation. The Monocle function clusterCells was used to detect cell clusters between
396 clusters. The Seurat function FindAllMarkers with default settings was used to find DEGs
397 upregulated in each cluster compared to the other cells. The top200 DEGs of cluster1 were used
398 for ordering cells, and the discriminative dimensionality reduction with trees (DDRTree) method
399 was used to reduce the data to two dimensions. The dynamic expression patterns with the
400 spermatogonial developmental trajectory of specific genes were visualized using the Monocle
401 function plot_genes_in_pseudotime and plot_pseudotime_heatmap. The procession data of the
402 adult human single-cell dataset was downloaded from Gene Expression Omnibus (GEO):
403 GSE112013 (Guo et al., 2018) and the UMI counts were analyzed using the Seurat R Package
404 (v.3.0.1) following the Seurat pipeline with the same parameters and functions as mentioned
405 previously. According to the known markers, the germ cells characterized was used for trajectory
406 analysis, and the single-cell pseudotime trajectory was constructed with the Monocle 2 package
407 (v2.12.0) as mentioned previously.
408
409 **CUT&Tag sequencing and analysis**
410 CUT&Tag assay was performed using CUT&Tag 2.0 High-Sensitivity Kit (Novoprotein scientific
411 Inc., Cat# N259-YH01). The detailed procedures were described in (Kaya-Okur et al., 2019; Wang
412 et al., 2021). In brief, cells were harvested by trypsin and enriched by ConA-magnetic beads.
413 10,000 cells were re-suspended in 100 mL Dig-wash Buffer (20 mM HEPES pH 7.5; 150 mM NaCl;

414 0.5 mM Spermidine; 13 Protease inhibitor cocktail; 0.05% Digitonin) containing 2 mM EDTA and a
415 1:100 dilution of primary FOXC2 antibody. The primary antibody was incubated overnight at 4°C.
416 Beads were washed in Dig-wash Buffer 3 times and incubated with secondary antibody for 1 hour
417 at a dilution of 1:200. After incubation, the beads were washed 3 times in Dig-Hisalt Buffer (0.05%
418 Digitonin, 20 mM HEPES, pH 7.5, 300 mM NaCl, 0.5 mM Spermidine, 13 Protease inhibitor
419 cocktail). Cells were incubated with proteinA-Tn5 transposome at 25°C for 1 hour and washed 3
420 times in Dig-Hisalt buffer to remove unbound proteinA-Tn5. Next, cells were re-suspended in
421 100mL Tagmentation buffer (10 mM MgCl2 in Dig-Hisalt Buffer) and incubated at 37°C for 1 hour.
422 The tagmentation was terminated by adding 2.25 mL of 0.5 M EDTA, 2.75 mL of 10% SDS and 0.5
423 mL of 20 mg/mL Proteinase K at 55°C for 1 hour. The DNA fragments were extracted by phenol
424 chloroform and used for sequencing on an Illumina HiSeq instrument (Illumina NovaSeq 6000) to
425 generate 2 × 150-bp paired-end reads following the manufacturer's instructions.
426 Raw reads were analyzed by removing low-quality or adaptor sequences using Trim_galore
427 (v0.5.0) and cleaned reads were mapped to the reference genome mm10 using Bowtie2 (v2.2.5).
428 We used MACS2 (v2.1.2) to call peaks found in different groups. Homer (v4.11.1) de novo motif
429 discovery tool was used for finding the binding motifs of Foxc2 with the findMotifsGenome.pl
430 command. The binding potential of candidate target genes at the binding motif was predicated
431 using the JASPAR Scan function (binding potential >0.8). The peaks filtered by fold change more
432 than 5 and transcription start site (TSS) less than 3000 bp were annotated by R package Chip
433 Seeker for gene category analysis. R package Cluster profiler was used for gene function
434 annotation such as KEGG and GO analysis.
435
436 **Enrichment analyses**
437 Gene Ontology (GO) and KEGG pathway enrichment analyses were conducted using the
438 ClusterProfiler package (v3.12.0) (Yu et al., 2012) and the ClueGO app (v2.5.7) in Cytoscape
439 (v3.8.1) with default settings and a p-value cut-off of 0.05. GSEA enrichment analysis was
440 assessed using the GSEA (v4.0.2) algorithm with MSigDB (v7.0) with default settings. The signaling
441 pathways enriched by niche-derived paracrine factors and undifferentiated SPG-derived
442 membrane proteins in the DEGs of the four samples were characterized. Then for each niche cell
443 type, the niche-derived signaling pathways in all four samples were crossed with the SSC-derived
444 signaling pathways to identify the candidate signaling pathways pivotal to SSCs maintenance.
445
446 **Transplantation assay**
447 The 8-week-old C57BL/6J WT mice were treated with busulfan (40 mg/kg) and used as recipient
448 mice 1 month later. SSCs were transplanted into the testis of recipient mice (1×10^3 cells/testis),
449 and two months after transplantation, the testes were harvested and observed under a
450 fluorescence microscope.
451
452 **Fluorescence-activated cell sorting (FACS)**
453 Single-cell suspensions were generated from testes or *in vitro* cultured SSCs. FACS was performed
454 using an SH800 machine (Sony Biotechnology) to isolate the GFP^+ cells. Briefly, the GFP^+ gating
455 area was based on the point of the fluorescence intensity axis where cells were considered as
456 being GFP^+, set based on the background fluorescence intensity of a non-transgenic control testis
457 cell population.
458
459 **Immunofluorescence**

460 Mouse testes were fixed in 4% Paraformaldehyde (PFA) at 4°C overnight, dehydrated, embedded
461 in paraffin, and cut into 5-μm thick sections. The rehydrated mouse or human testis sections were
462 subjected to antigen retrieval, blocked in 5% BSA with 0.1% Triton X-100, and incubated with
463 primary antibody (Materials and methods—source data 1) at 4°C overnight, including the germ cell
464 marker DDX4, undifferentiated spermatogonia markers ZBTB16, LIN28A, ECAD (Tokuda et al.,
465 2007), GFRA1, EOMES, PAX7, progenitor marker NEUROG3, and spermatocyte marker SYCP3
466 (Yuan et al., 2000). After three 5-min washes in PBS, the sections were incubated with secondary
467 antibodies (Materials and methods—source data 1) and DAPI (Sigma) at 37°C for 1 hour. After
468 three 5-min washes in PBS, coverslips were then mounted on glass slides using anti-quencher
469 fluorescence decay (Solarbio). Images were captured using a Zeiss 780 laser-scanning confocal
470 microscope. Whole-mount immunofluorescence of seminiferous tubules was performed as
471 previously described (Di Persio et al., 2017). Briefly, seminiferous tubules were disentangled from
472 testicular biopsies and immediately fixed in 4% PFA at 4°C for 12 hours. After fixation, the
473 seminiferous tubules were permeabilized with 0.5% Triton X-100 in PBS and treated with 5% BSA
474 in PBS overnight at 4°C. After three 30-min washes, the seminiferous tubules were incubated with
475 primary antibody (Materials and methods—source data 1) overnight at 4°C. After three 30-min
476 washes, the seminiferous tubules were incubated with species-specific secondary antibodies and
477 DAPI at 4°C for 12 hours. After three 30-min washes, the seminiferous tubules were mounted on
478 slides with anti-quencher fluorescence decay (Solarbio) and observed with a Zeiss 780 laser-
479 scanning confocal microscope.
480
481 **RNA isolation and quantitative RT-PCR analysis**
482 Total RNA was extracted from the testes or cultured cells using the RNeasy kit (Qiagen), reverse-
483 transcribed using RevertAid First Strand cDNA Synthesis kit (Thermo), and processed for qRT-
484 PCR using PowerUp SYBR Green Master Mix (Applied Biosystems) and a LightCycler 480 system
485 (Roche) with gene-specific primers (Materials and methods—source data 1). Reactions were run
486 in triplicate and the mRNA levels were normalized to Gapdh and quantified using the delta-delta Ct
487 method. The values shown are mean ± s.e.m. from three biological replicates.
488
489 **Tamoxifen inducible**
490 According to a previous report for activation of iCre (M. Sharma et al., 2019), the mice were fed
491 with TD.130859 (TAM diet) for three days. The food was formulated for 400 mg tamoxifen citrate
492 per kg diet, which would provide ~40 mg tamoxifen per kg body weight per day.
493 *Analyses of cyst length.* The cyst length was obtained according to the previous report (Nakagawa
494 et al., 2010). Briefly, to determine the cyst length, after immunofluorescence staining with anti-E-
495 CAD antibody, the whole mount seminiferous tubule specimens were observed under a
496 fluorescence microscope. The E-CAD staining coupled with staining for FOXC2 enabled us to
497 reliably identify syncytial cysts of $FOXC2^+$ cells.
498
499 **Analyses of cell density**
500 The cell density was counted according to a previous report (Tegelenbosch & de Rooij, 1993).
501 Briefly, the densities of the $ZBTB16^+$, $GFRA1^+$, $LIN28A^+$, or $FOXC2^+$ cells were measured on the
502 seminiferous tubules with whole-mount staining, the numbers of which per 1000 Sertoli cells were
503 determined.
504
505 **Sperm counts**

506 Total sperm counts were obtained according to the previous report (Roy et al., 2007). Briefly,
507 epididymal caput and cauda were minced and incubated in prewarmed M16 medium (Sigma-
508 Aldrich) at 37°C in air containing 5% CO_2 for 30 min to allow the sperm to swim out. Then, the
509 sperm were diluted in water and counted using a hemocytometer.
510
511 **Histology, evaluation of degenerating tubules**
512 Testes of WT and mutant mice were fixed with PFA fixative and processed for paraffin-embedded
513 section preparation (5 μm thick) and hematoxylin and eosin staining, according to standard
514 procedures. The percentage of degenerating seminiferous tubules was calculated based on the
515 cross-sections of seminiferous tubules (n > 200) that appeared on one transverse section for each
516 testis. In normal (WT) mouse testes, four generations of germ cells, each synchronously
517 progressing through spermatogenesis, form cellular associations of fixed composition (called
518 seminiferous epithelial stages). In the testes of *Foxc2*$^{f/-}$*;Ddx4*$^{Cre/+}$ mice, a few tubule cross-sections
519 lacked one or more out of the four germ cell layers, which was defined as "degenerative tubules"
520 in this study.
521
522 **Statistical analysis**
523 All statistical analyses were performed using GraphPad Prism (v7.0). All experiments were
524 repeated at least three times, and data for evaluated parameters are reported as mean ± s.e.m.
525 The p-values were obtained using two-tailed unpaired Student's t-tests or one-way ANOVA
526 followed by Tukey test (ns represents p-value > 0.05, * represents p-value < 0.05, ** represents p-
527 value < 0.01, *** represents p-value < 0.001, and **** represents p-value < 0.0001).
528
529 **Acknowledgments**
530 This work was supported by the National Key Research and Development Program of China grant
531 (2022YFA0806302, 2018YFC1003500, 2019YFA0801800), CAMS Innovation Fund for Medical
532 Sciences (CIFMS, 2021-I2M-1-019, 2017-I2M-3-009), National Natural Science Foundation of
533 China grant (92268111, 31970794, 32000586, 31725013, 32200646), and State Key Laboratory
534 Special fund from the Ministry of Science grant (2060204).
535
536 **Materials and methods—source data 1**. Excel spreadsheet with the primers and antibodies
537 used in this study.
538
539 **Data Availability.** All data are available in the main text or supplementary materials. The scRNA-
540 seq and CUT&Tag sequencing data produced in this study have been uploaded to the GEO
541 (https://www.ncbi.nlm.nih.gov/geo) with accession codes GSE183163, GSE180729, and
542 GSE180926. The expression of FOXC2 in adult human testis used the scRNA-seq dataset
543 GSE112013 from previously published "The Human Testis Cell Atlas via Single-cell RNA-seq" by
544 Jingtao Guo (https://www.ncbi.nlm.nih.gov/geo/query/acc.cgi?acc=GSE112013) (Guo et al., 2018).
545 All of the R packages were available online and the code was used according to respective R
546 packages documentation as described in the Methods. The MSigDB (v.7.0) used in this study is
547 available at https://www.gsea-msigdb.org/gsea/msigdb.
548

549 **Figures**

550

551 **Figure 1** with 2 supplements

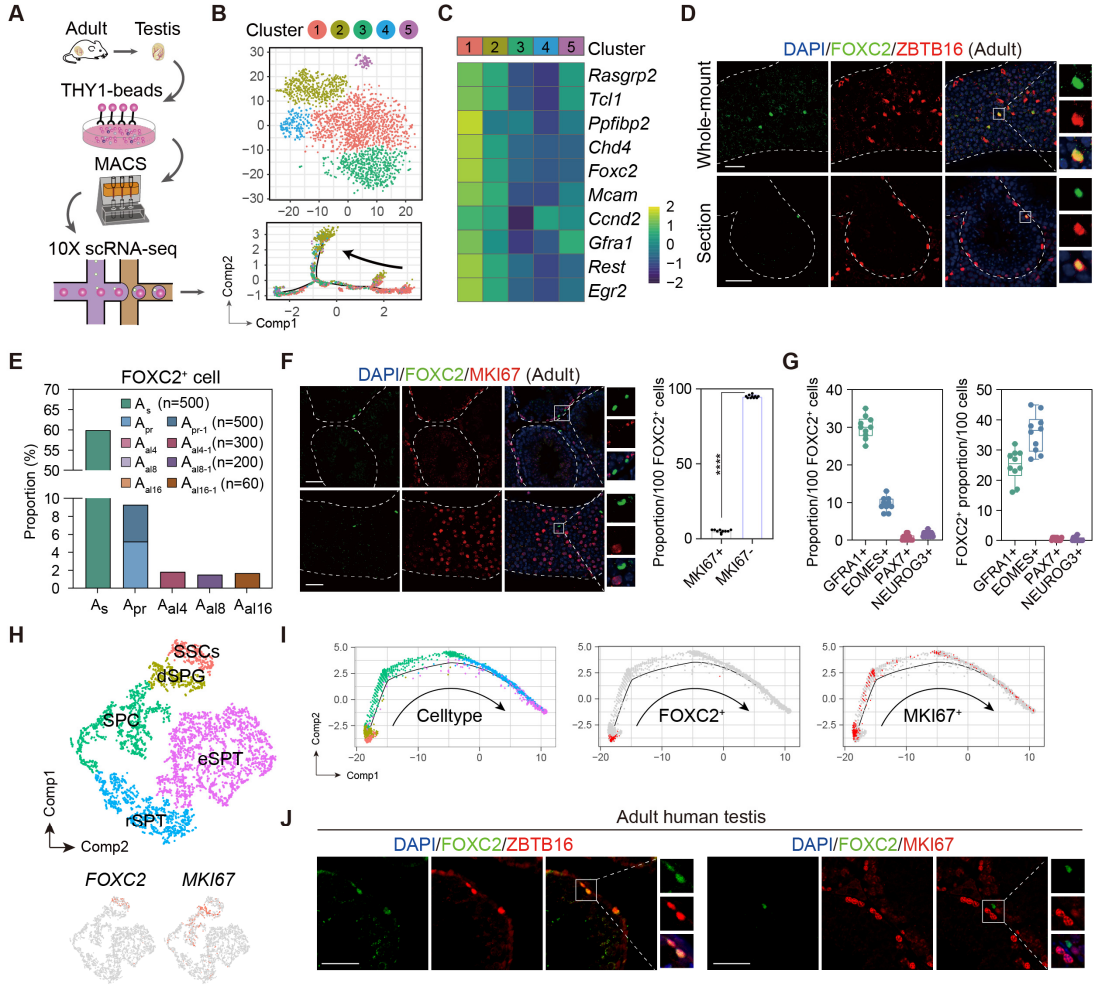

552

553 **Identification of the FOXC2⁺ SSCs in adult mouse and human testis.** (**A**) Schematic illustration
554 of the single-cell analysis workflow. (**B**) t-SNE plot and developmental trajectory of all uSPG,
555 colored by cluster. (**C**) Heatmap of the Top10 DEGs in Cluster1. (**D**) Immunostaining for ZBTB16
556 (red), FOXC2 (green), and DAPI (blue) in testicular paraffin sections from wild-type adult C57 mice.
557 Scale bar, 50 μm; C57, C57BL/6J. (**E**) The proportion of FOXC2⁺ cells in different uSPG subtypes.
558 (**F**) Immunostainings for MKI67 (red), FOXC2 (green), and DAPI (blue) in adult mice testis and the
559 proportion of MKI67⁺ cells in FOXC2⁺ population (n=10). Scale bar, 50 μm; values, mean ± s.e.m.;
560 p-values were obtained using two-tailed t-tests (****p-value < 0.0001). (**G**) The co-expression
561 proportion between the FOXC2 and differential known SSCs makers (n=10). (**H**) t-SNE plot of germ
562 cells in adult human testis (GSE112013), colored by germ cell type. Feature plot showing the
563 expression patterns of FOXC2 and MKI67 in human germ cells. (**I**) The developmental trajectory of
564 the human germ cells, colored by germ cell type, FOXC2 expression cells (red), or MKI67
565 expression cells (red). (**J**) Immunostaining for ZBTB16/MKI67 (red), FOXC2 (green), and DAPI
566 (blue) in testicular paraffin sections from adult humans.

567 **Figure 1—figure supplement 1**

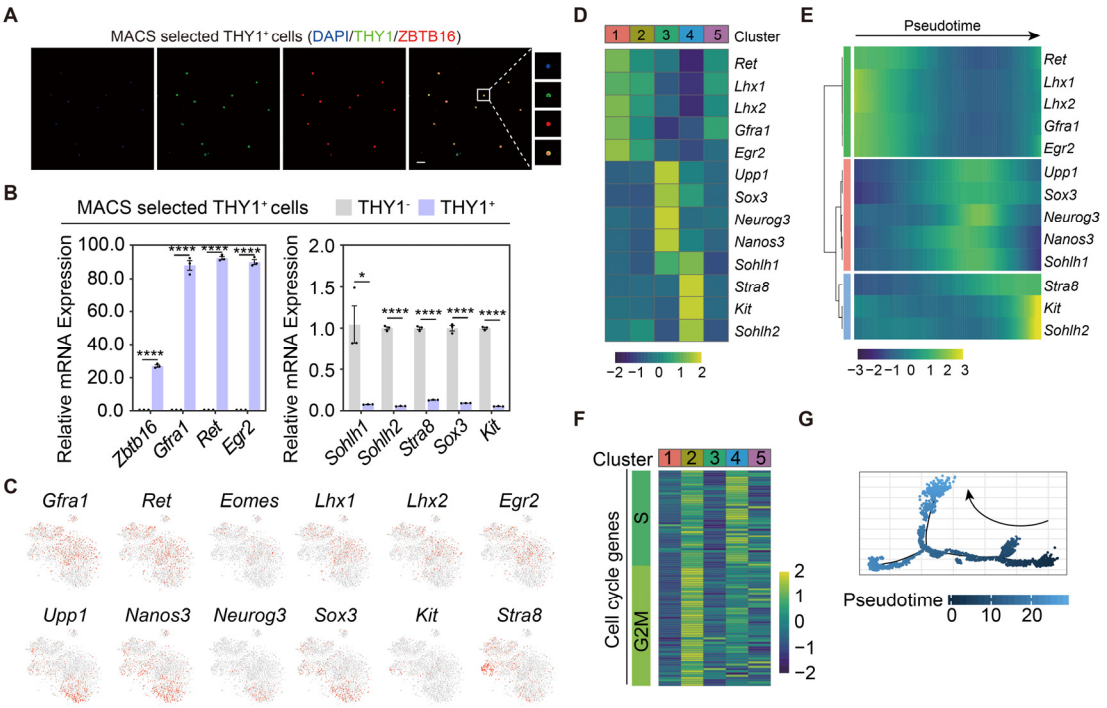

568
569 **Validation and characterization of the MACS-sorted THY1⁺ uSPG from wild-type adult C57**
570 **mice.** (**A**) Immunostainings of DAPI (blue), THY1 (green), and ZBTB16 (red) in the MACS-sorted
571 THY1⁺ cells (n=5). Scale bar, 50 μm. (**B**) Quantitative RT-PCR analysis of uSPG and dSPG
572 markers expressed in the MACS-sorted THY1⁺ cells (n=3). Values, mean ± s.e.m.; p-values were
573 obtained using two-tailed t-tests (ns > 0.05, *p-value < 0.05, **p-value < 0.01, ***p-value < 0.001,
574 ****p-value < 0.0001). (**C**) Feature plots showing the expression pattern of classic SPG markers
575 (stemness and differentiation). (**D**) Heatmap showing the expression pattern of markers for SPG in
576 different clusters. (**E**) Expression pattern dynamics of the SPG markers with pseudotime
577 progression. (**F**) Heatmap showing the expression pattern of markers for cell cycle phase in
578 different clusters. (**G**) The developmental trajectory of the overall SPG, colored by pseudotime.
579
580
581

582 **Figure 1—figure supplement 2**

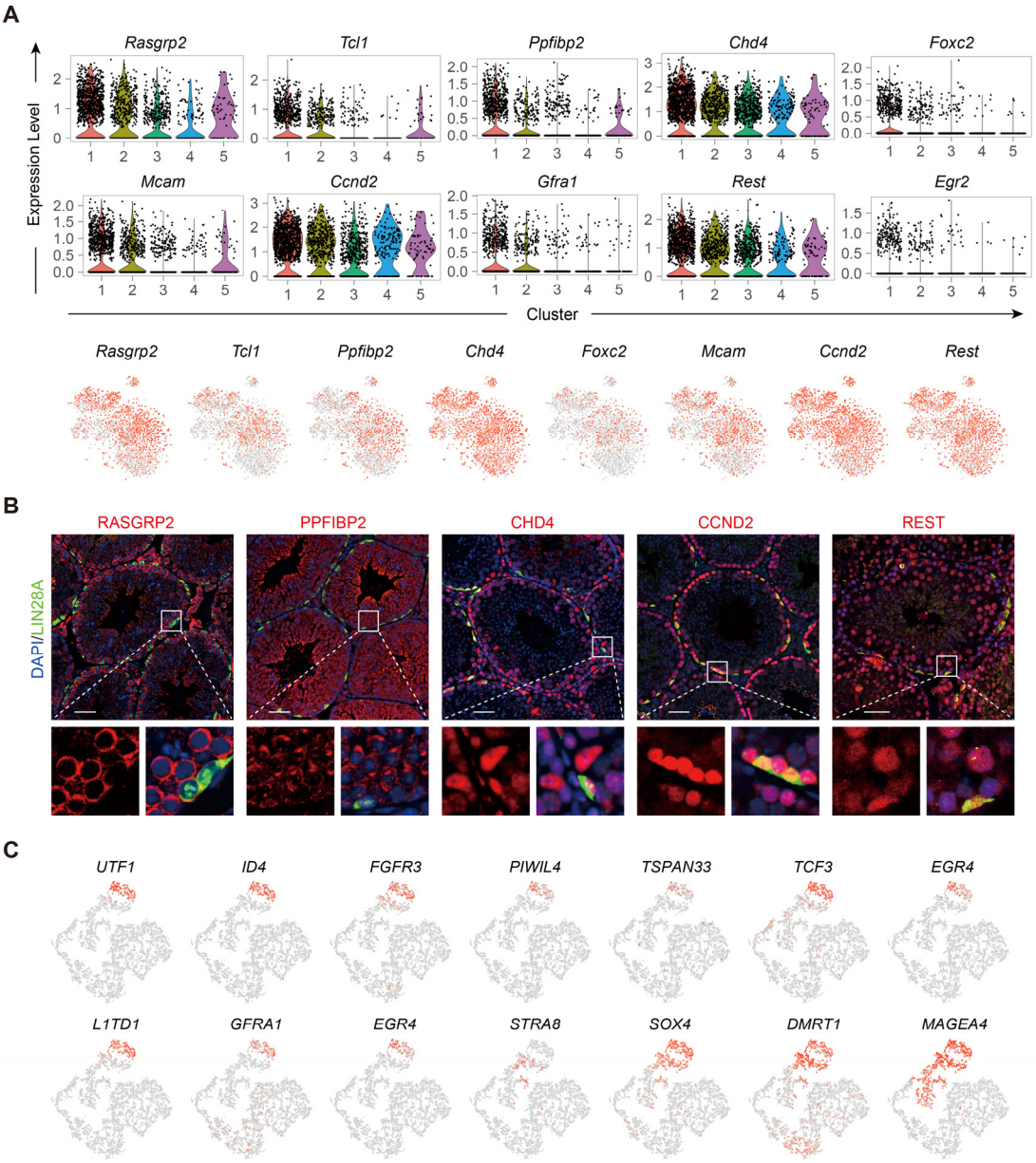

583

584 **Expression of top10 DEGs of Cluster1 in Figure 1B and classic SSC and SPG markers in**
585 **adult human germ cells.** (**A**) Feature plots and violin plots of the Top10 DEGs of Cluster1. (**B**)
586 Immunostainings for LIN28A (red), DAPI (blue), and newly-found markers (green) in testicular
587 paraffin sections from adult mice. Scale bar, 50 μm. (**C**) Feature plots showing the expression
588 pattern of classic SSCs and SPG markers in adult human germ cells.

589

590 **Figure 1—source data 1**. Excel spreadsheet with the list of the top30 differentially expressed
591 genes of different clusters.

592

593 **Figure 2** with 1 supplement

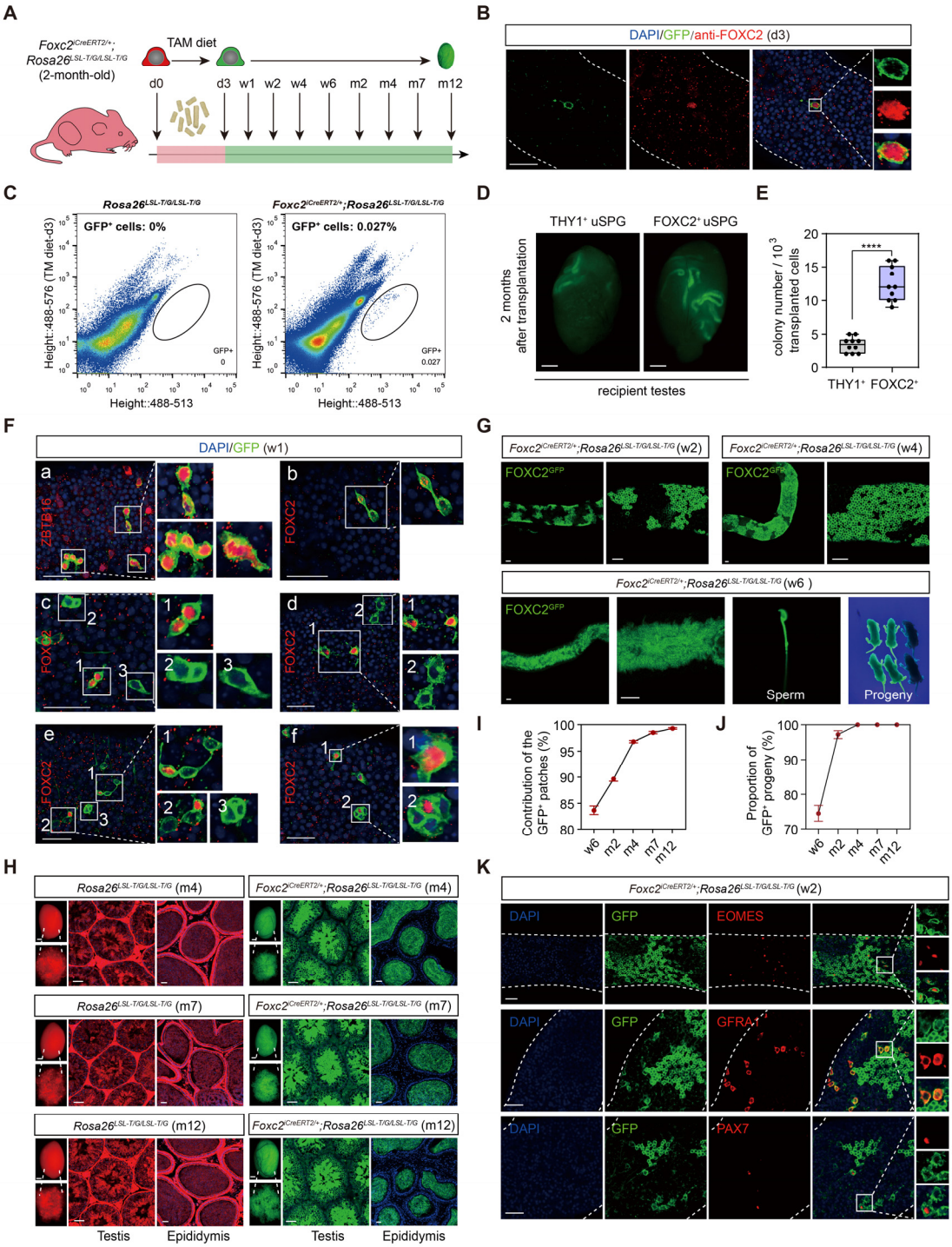

594

595 **Lineage tracing and functional validation of FOXC2⁺ SSCs in *Foxc2*$^{iCreERT2/+}$;*Rosa26*$^{LSL\text{-}T/G/LSL\text{-}T/G}$ mice.** (**A**) Schematic illustration of the lineage tracing workflow for FOXC2⁺ cells. (**B**)
596 Immunostainings for DAPI (blue) and FOXC2 (red) at day 3 post TAM induction. Scale bar, 50 μm;
597 d, day. (**C**) FACS analysis of GFP⁺ populations derived from *Rosa26*$^{LSL\text{-}T/G/LSL\text{-}T/G}$ or
598

599 *Foxc2*$^{iCreERT2/+}$;*Rosa26*$^{LSL\text{-}T/G/LSL\text{-}T/G}$ mice at day 3 post TAM induction. (**D**, **E**) The recipient mice
600 testes (**D**) and colony numbers (**E**) 2 months after transplantation (n=10) of the FACS-sorted GFP^{+}
601 cells from the *Foxc2*$^{iCreERT2/+}$;*Rosa26*$^{LSL\text{-}T/G/LSL\text{-}T/G}$ mice 3 days after TAM diet and the FACS-sorted
602 THY1^{+} cells from adult mice. Scale bar, 1 mm; values, mean ± s.e.m.; p-values were obtained using
603 two-tailed t-tests (****p-value < 0.0001). (**F**) Immunostaining for DAPI (blue), ZBTB16/FOXC2 (red),
604 and GFP (green) at week 1 post TAM induction (scale bar, 50 μm). (**G**) Seminiferous tubules of
605 *Foxc2*$^{iCreERT2/+}$;*Rosa26*$^{LSL\text{-}T/G/LSL\text{-}T/G}$ mice 2, 4, and 6 weeks post TAM induction. Scale bar, 50 μm.
606 (**H**) Testes (scale bar, 1 mm), seminiferous tubules, and epididymis (scale bar, 50 μm) at month 4,
607 7, and 12 post TAM induction in *Foxc2*$^{iCreERT2/+}$;*Rosa26*$^{LSL\text{-}T/G/LSL\text{-}T/G}$ mice. (**I**, **J**) The GFP^{+} patches
608 (**I**) and progeny (**J**) population dynamics (n=10). Values, mean ± s.e.m. (**K**) Immunostainings for
609 DAPI (blue), EOMES (red), GFRA1 (red), or PAX7 (red) in GFP^{+} population at week 2 post TAM
610 induction. Scale bar, 50 μm.
611
612

613 **Figure 2—figure supplement 1**

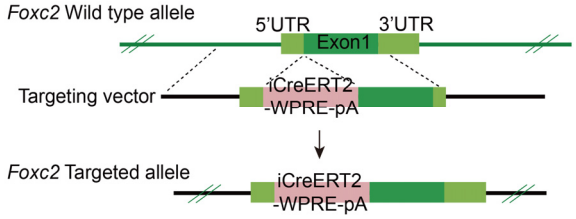

614

615 **Construction of the *Foxc2*^{iCreERt2} mice.**

616 **Figure 3** with 1 supplement

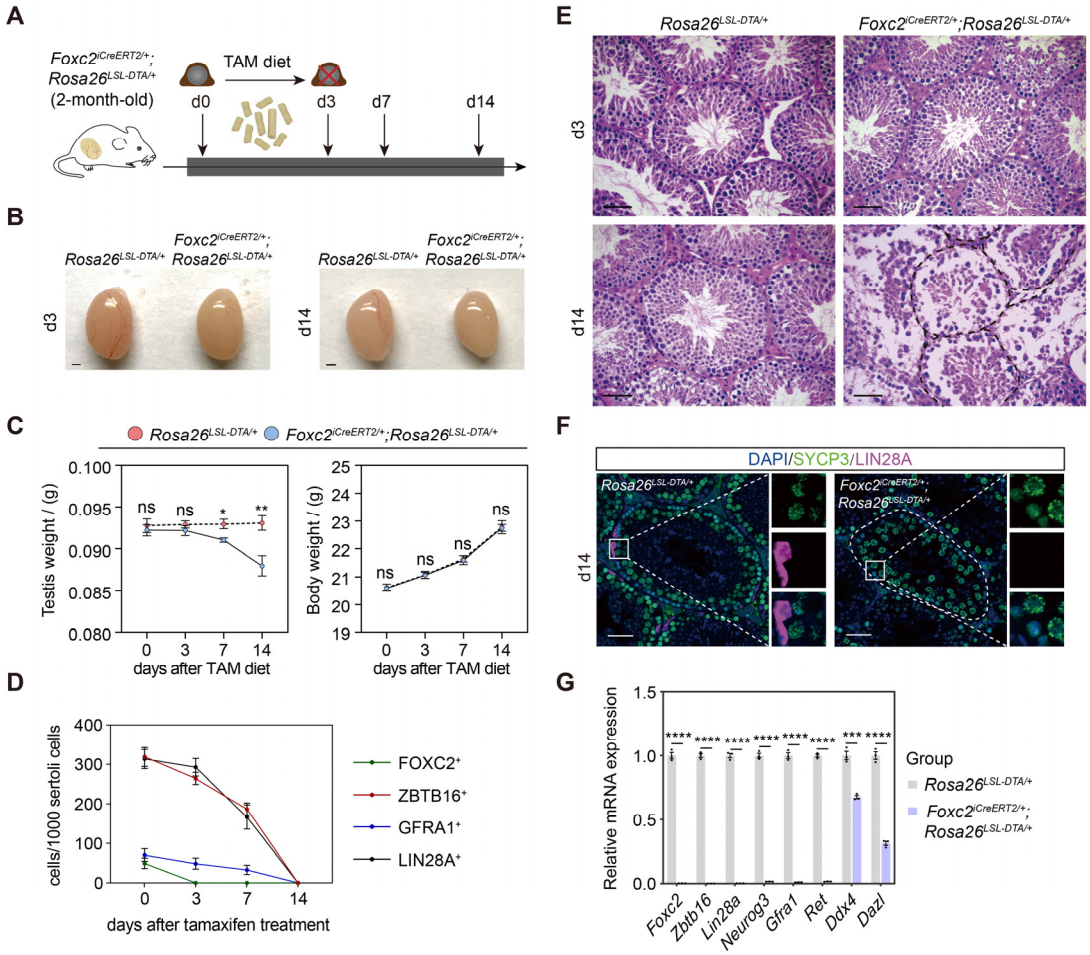

617

618 **Specific ablation of FOXC2⁺ SSCs and phenotypic validation in *Foxc2*$^{iCreERT2/+}$;*Rosa26*$^{LSL\text{-}DTA/+}$**
619 **mice.** (**A**) Schematic illustration of the lineage tracing workflow for FOXC2⁺ cells. (**B-D**) Phenotypic
620 validation of the *Rosa26*$^{LSL\text{-}DTA/+}$ and *Foxc2*$^{iCreERT2/+}$;*Rosa26*$^{LSL\text{-}DTA/+}$ mice (n=5) for testes size (**B**),
621 testis weight and body weight (**C**), and HE-staining of the testes (**D**). Scale bars in (**B**), 1 mm; in
622 (**D**), 50 µm; d, day; values were mean ± s.e.m.; p-values were obtained using two-tailed t-tests
623 (ns > 0.05, *p-value < 0.05, **p-value < 0.01). (**E**) ZBTB16⁺, GFRA1⁺, LIN28A⁺, and FOXC2⁺ SPG
624 populations dynamics. Values, mean ± s.e.m. (n=10); p-values were obtained using one-way
625 ANOVA followed by Tukey test (ns > 0.05, *p-value < 0.05, **p-value < 0.01, ****p-value < 0.0001).
626 (**F**) Immunostainings for DAPI (blue), SYCP3 (green), and LIN28A (magenta) at day 14 post TAM
627 induction. d, day; scale bar, 50 µm. (**G**) Quantitative RT-PCR analysis of SPG markers expression
628 in the testes of the *Rosa26*$^{LSL\text{-}DTA/+}$ and *Foxc2*$^{iCreERT2/+}$;*Rosa26*$^{LSL\text{-}DTA/+}$ mice (n=3). Values, mean ±
629 s.e.m.; p-values were obtained using two-tailed t-tests (***p-value < 0.001, ****p-value < 0.0001).
630
631

632 **Figure 3—figure supplement 1**

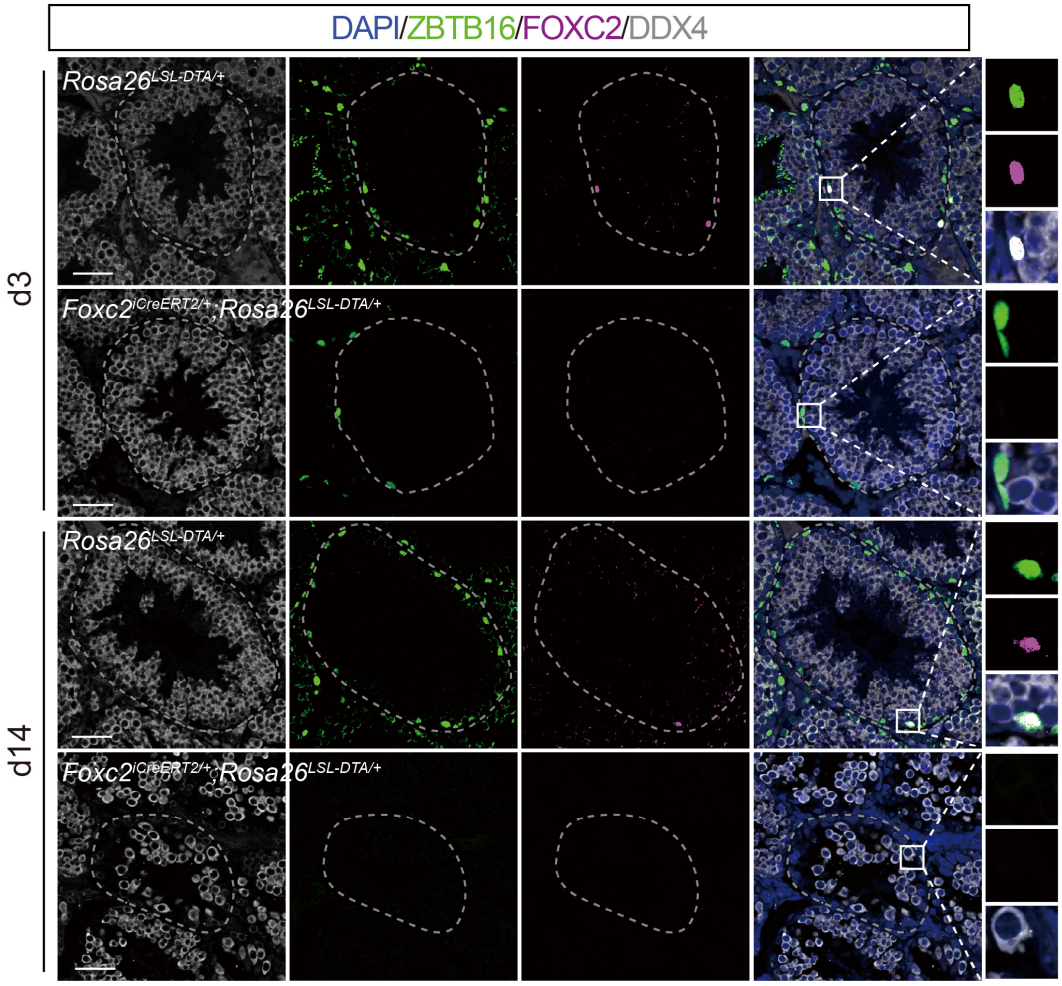

633
634 **Depletion of uSPG pool in *Foxc2*$^{iCreERT2/+}$;*Rosa26*$^{LSL-DTA/+}$ mice 14 days after specific ablation**
635 **of FOXC2^{+} SSCs.** Immunostainings for DAPI (blue), DDX4 (white), ZBTB16 (green), and FOXC2
636 (magenta) at day 3 and day 14 post TAM induction in *Foxc2*$^{iCreERT2/+}$;*Rosa26*$^{LSL-DTA/+}$ mice (scale
637 bar, 50 μm).
638

Figure 4

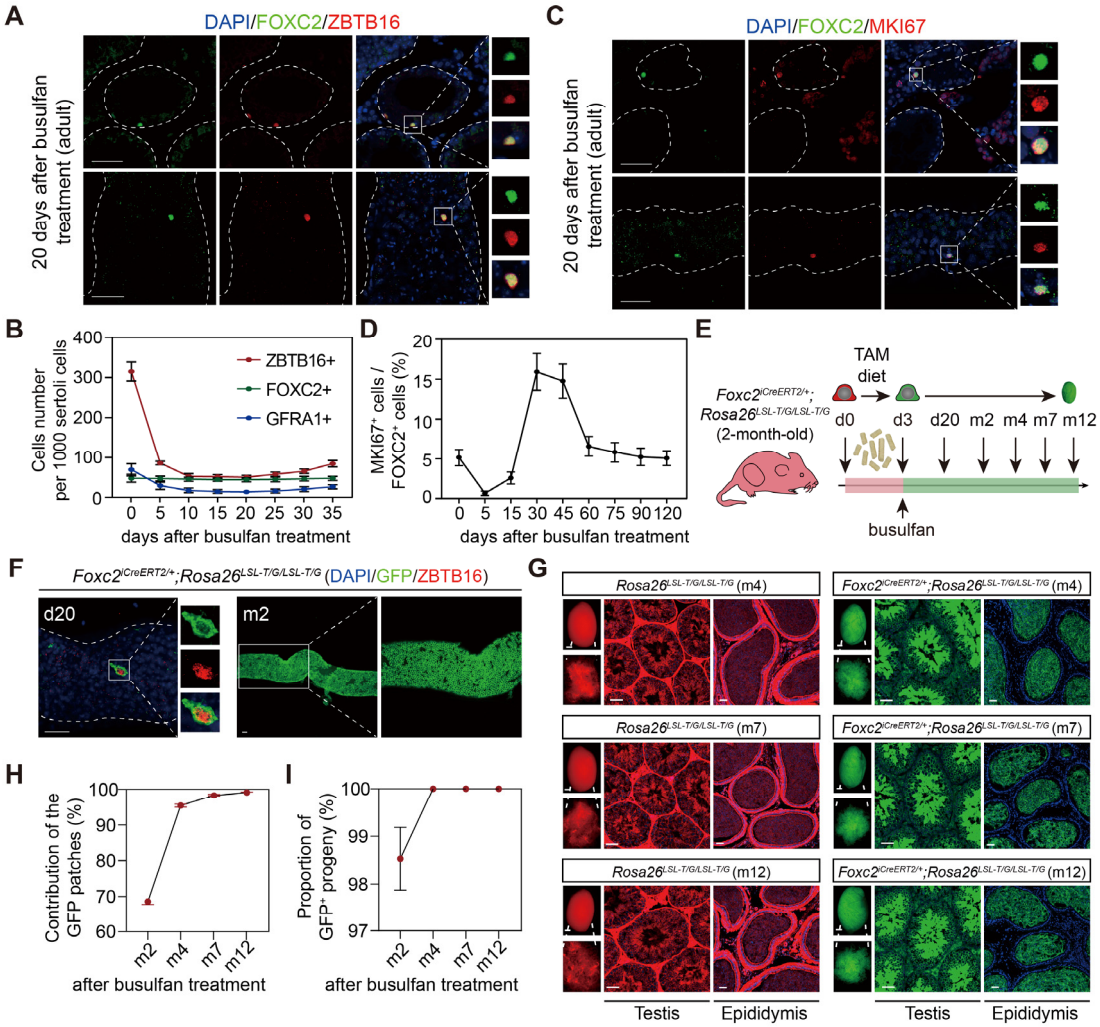

FOXC2⁺ SSCs are critical for germline regeneration. (**A**) Co-immunostaining of FOXC2 (green) with ZBTB16 (red) in seminiferous tubules of the adult testes at day 20 post busulfan treatment. Scale bar, 50 μm. (**B**) ZBTB16⁺, GFRA1⁺, and FOXC2⁺ population dynamics after busulfan treatment (20 mg/kg, n=10). (**C**) Co-immunostaining of FOXC2 (green) with MKI67 (red) in seminiferous tubules of the adult testes at day 20 post busulfan treatment. Scale bar, 50 μm. (**D**) MKI67⁺FOXC2⁺ proportions in relation to the whole FOXC2⁺ population at different time points after busulfan treatment (n=4). (**E**) Schematic illustration for lineage tracing of FOXC2⁺ cell after busulfan treatment. (**F**) Lineage tracing of the GFP⁺ cells at day 20 and month 2 after busulfan treatment (scale bar, 50 μm). (**G**) The testes (scale bar, 1 mm), seminiferous tubules, and epididymis (scale bar, 50 μm) at month 4, 7, and 12 post TAM induction and busulfan injection. m, month. (**H**, **I**) The proportion dynamics of GFP patches (**H**) and GFP⁺ progenies (**I**). Values, mean ± s.e.m. (n=10). w, week; m, month.

653 **Figure 5** with 1 supplement

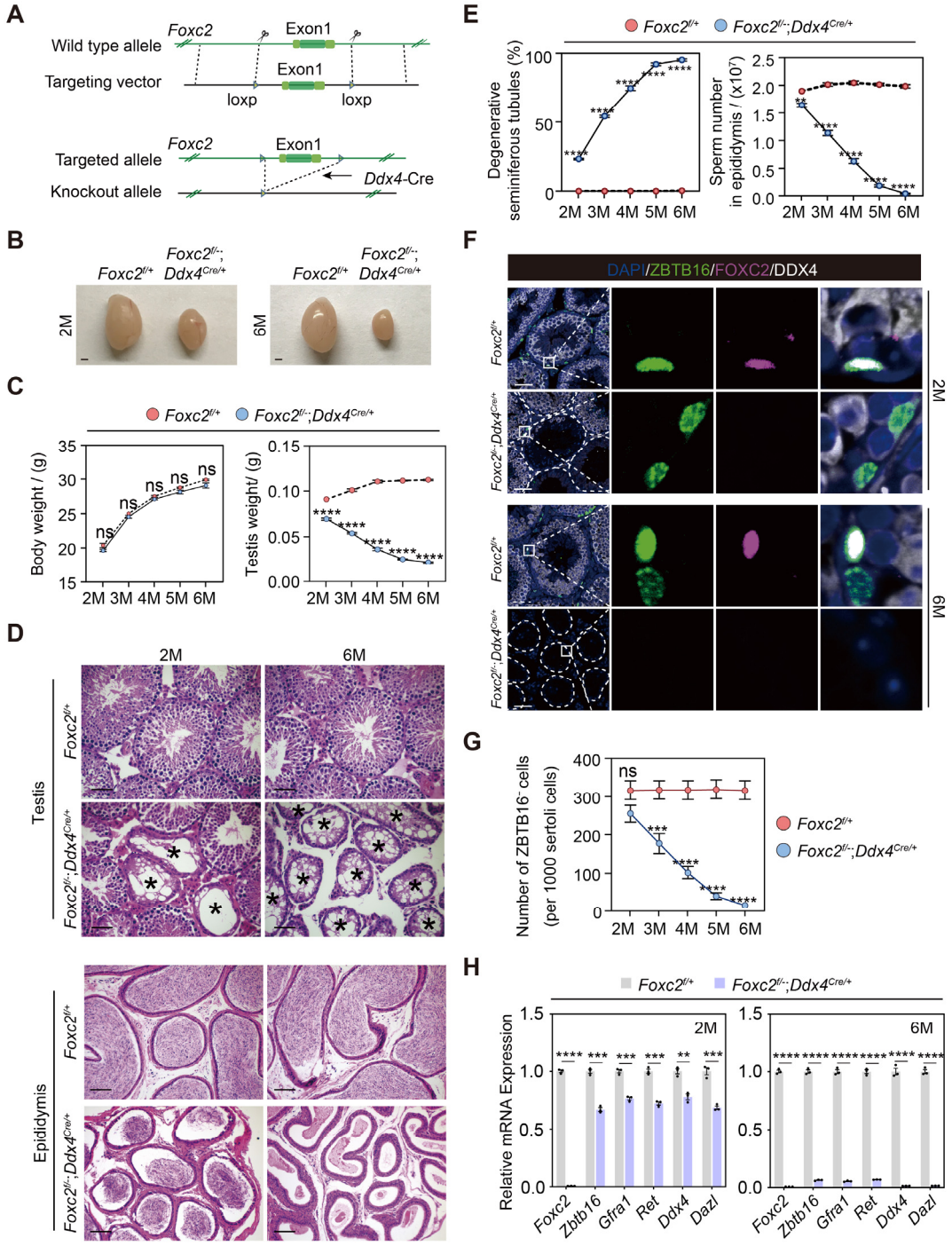

654

655 **Spermatogenesis exhaustion in the adult *Foxc2$^{f/-}$;Ddx4$^{Cre/+}$* mice.** (**A**) Construction of the
656 *Foxc2$^{f/-}$;Ddx4$^{Cre/+}$* mice. (**B**) The testes size of the *Foxc2$^{f/-}$;Ddx4$^{Cre/+}$* mice. Scale bar, 1mm; M,
657 month. (**C**) Body weight and testis weight of the *Foxc2$^{f/-}$;Ddx4$^{Cre/+}$* mice at different age (n=5). M,
658 month; values, mean ± s.e.m.; p-values were obtained using two-tailed t-tests (ns > 0.05, ****p-
659 value < 0.0001). (**D**) HE-staining of the testis and epididymis. Scale bar, 50 μm; M, month. (**E**)

Estimation of degenerative tubules and sperm counts in cauda epididymis of the *Foxc2*$^{f/+}$ and *Foxc2*$^{f/-}$*;Ddx4*$^{Cre/+}$ mice with age (n=5). Values, mean ± s.e.m.; p-values were obtained using two-tailed t-tests (**p-value < 0.01, ****p-value < 0.0001). (**F**) Immunostainings for DAPI (blue), ZBTB16 (green), FOXC2 (magenta), and DDX4 (white) in the seminiferous tubules of the *Foxc2*$^{f/+}$ and *Foxc2*$^{f/-}$*;Ddx4*$^{Cre/+}$ mice. Scale bar, 50 µm. (**G**) Estimation of ZBTB16^{+} uSPG number in the *Foxc2*$^{f/+}$ and *Foxc2*$^{f/-}$*;Ddx4*$^{Cre/+}$ mice with age (n=5). Values, mean ± s.e.m.; p-values were obtained using two-tailed t-tests (ns > 0.05, ***p-value < 0.001, ****p-value < 0.0001). (**H**) Quantitative RT-PCR analysis of the uSPG and germ cell markers expressed in the testis of the *Foxc2*$^{f/+}$ and *Foxc2*$^{f/-}$*;Ddx4*$^{Cre/+}$ mice (n=3). M, month; values, mean ± s.e.m.; p-values were obtained using two-tailed t-tests (**p-value < 0.01, ***p-value < 0.001, ****p-value < 0.0001).

672 **Figure 5—figure supplement 1**

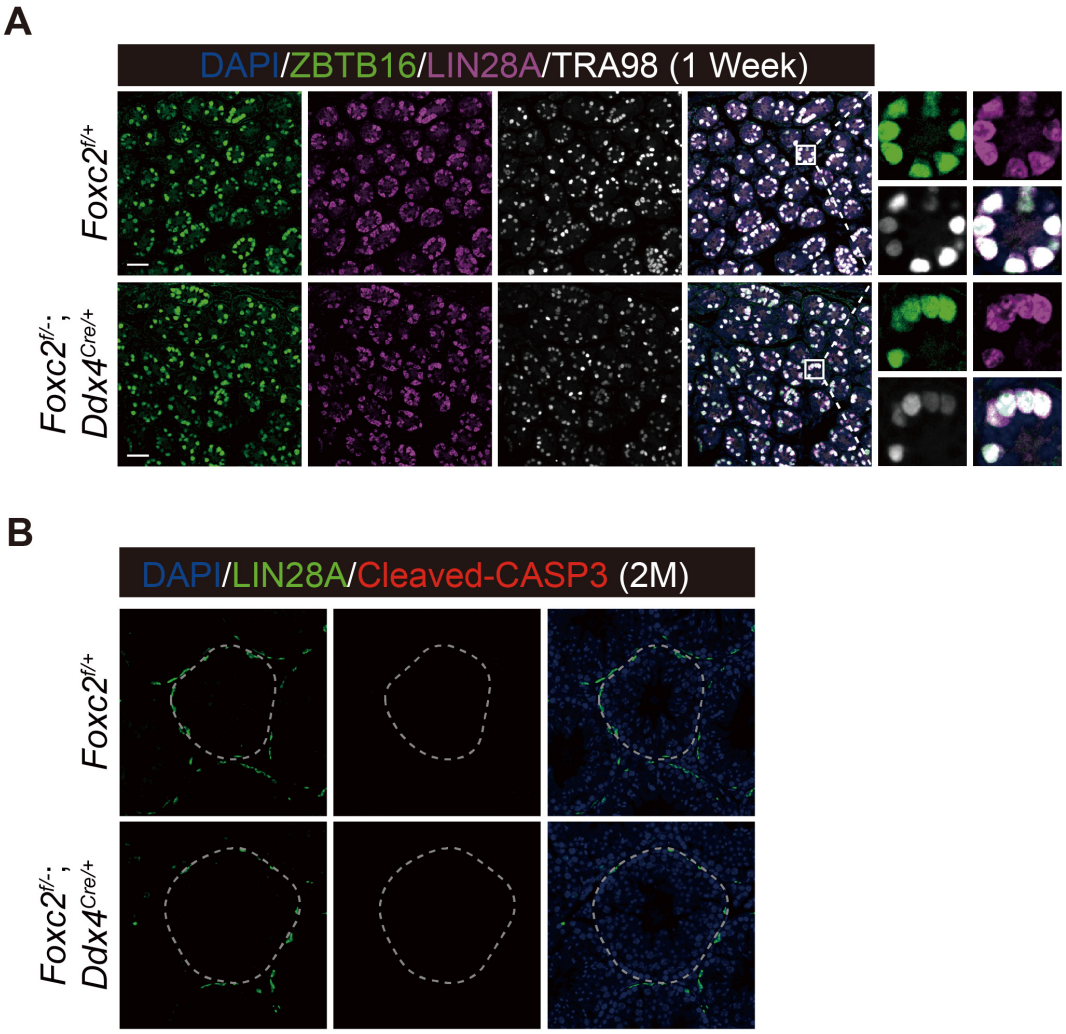

673
674 **Phenotypic validation of the *Foxc2$^{f/-}$;Ddx4$^{Cre/+}$* mice.** (**A**) Immunostainings for DAPI (blue),
675 ZBTB16 (green), LIN28A (magenta), and TRA98 (white) in seminiferous tubules of 1-week-old
676 *Foxc2$^{f/+}$* and *Foxc2$^{f/-}$;Ddx4$^{Cre/+}$* mice. Scale bar, 50 μm. (**B**) Immunostainings for DAPI (blue),
677 LIN28A (green), and Cleaved-CASP3 (red) in seminiferous of the *Foxc2$^{f/+}$* and *Foxc2$^{f/-}$;Ddx4$^{Cre/+}$*
678 mice (2-month-old). M, month; scale bar, 50 μm.

679 **Figure 6** with 2 supplements

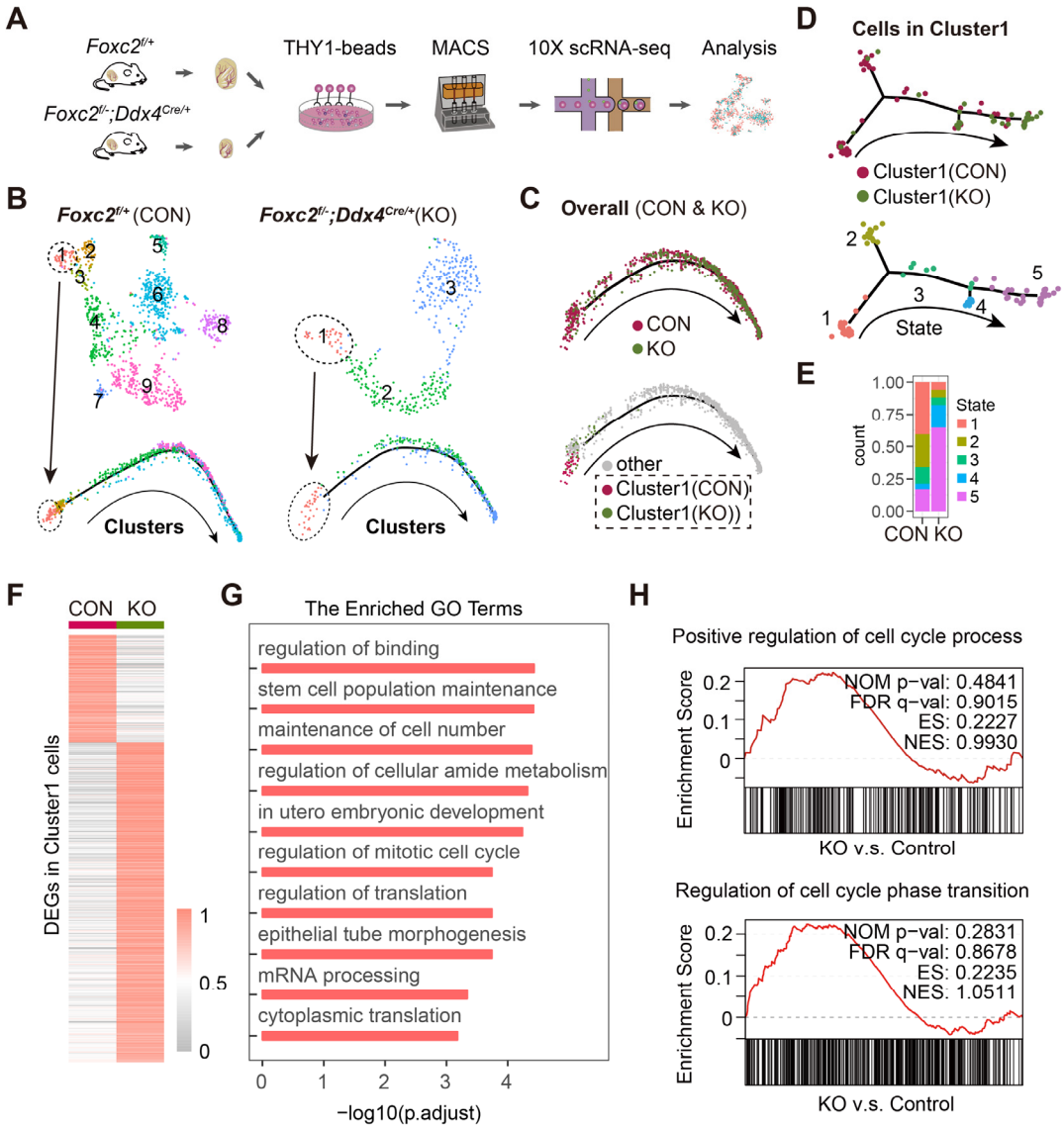

680

681 **scRNA-seq analysis of THY1⁺ uSPG in *Foxc2*$^{f/+}$ and *Foxc2*$^{f/-}$;*Ddx4*$^{Cre/+}$ mice.** (**A**) Schematic
682 illustration of the scRNA-seq workflow. (**B**) t-SNE plot and developmental trajectory of uSPG from
683 *Foxc2*$^{f/+}$ and *Foxc2*$^{f/-}$;*Ddx4*$^{Cre/+}$ mice respectively, colored by cluster. (**C**) Developmental trajectories
684 of uSPG from *Foxc2*$^{f/+}$ and *Foxc2*$^{f/-}$;*Ddx4*$^{Cre/+}$ mice, colored by sample or derivation. (**D**)
685 Developmental trajectories of the cells in Cluster1 from *Foxc2*$^{f/+}$ (CON) and *Foxc2*$^{f/-}$;*Ddx4*$^{Cre/+}$ (KO)
686 mice, colored by derivation or developmental state. (**E**) The Cluster1 cells proportion of each state
687 in CON and KO mice. (**F**) Heatmap showing the DEGs in the Cluster1 cells from the
688 *Foxc2*$^{f/-}$;*Ddx4*$^{Cre/+}$ mice compared with the *Foxc2*$^{f/+}$ mice. (**G**) Top GO terms enrichment by the
689 down-regulated DEGs in KO mice. (**H**) Gene set enrichment analysis (GSEA) of the Cluster1 cells
690 (*Foxc2*$^{f/-}$;*Ddx4*$^{Cre/+}$ v.s. *Foxc2*$^{f/+}$ mice). NOM, nominal; FDR, false discovery rate; ES, enrichment
691 score; NES, normalized enrichment score.

692 **Figure 6—figure supplement 1**

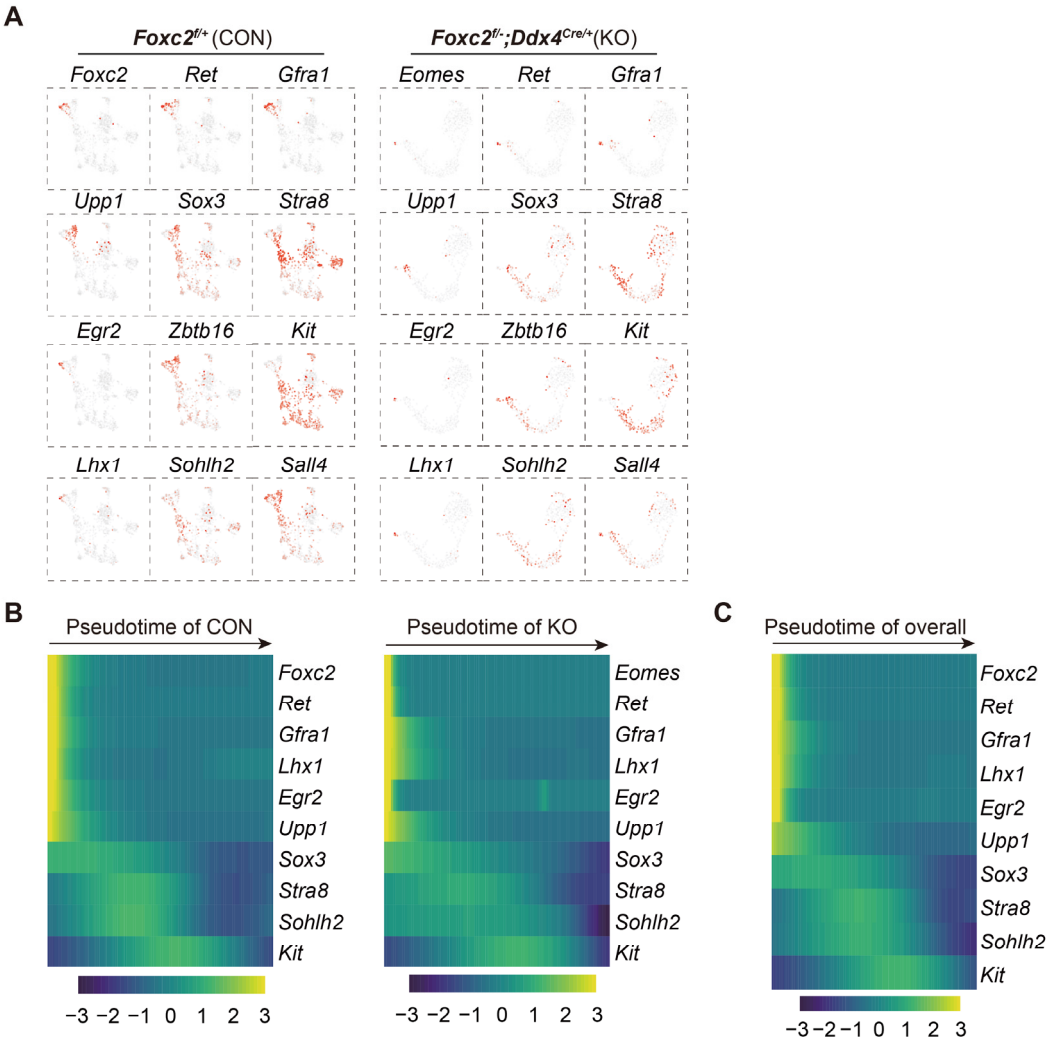

693
694 **scRNA-seq analysis of THY1⁺ uSPG in adult *Foxc2*$^{f/+}$ and *Foxc2*$^{f/-}$;*Ddx4*$^{Cre/+}$ mice.** (**A**) Feature
695 plots of classic SPG markers for uSPG in adult *Foxc2*$^{f/+}$ or *Foxc2*$^{f/-}$;*Ddx4*$^{Cre/+}$ mice. (**B**) Expression
696 dynamics of SPG markers with pseudotime progression for uSPG from *Foxc2*$^{f/+}$ or *Foxc2*$^{f/-}$;*Ddx4*$^{Cre/+}$
697 mice respectively. (**C**) Expression dynamics of SPG markers with pseudotime progression for
698 overall uSPG from *Foxc2*$^{f/+}$ and *Foxc2*$^{f/-}$;*Ddx4*$^{Cre/+}$ mice.
699
700

701 **Figure 6—figure supplement 2**

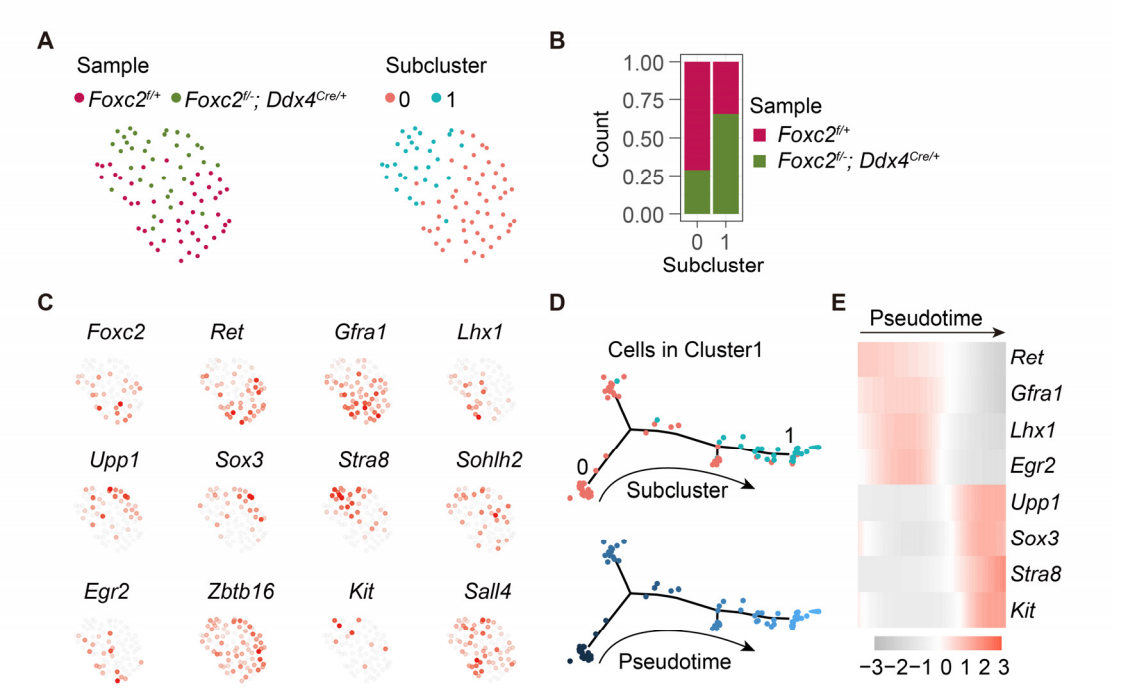

702
703 **Re-cluster and developmental trajectory analysis of cells in Cluster1 derived from adult**
704 ***Foxc2*$^{f/+}$ and *Foxc2*$^{f/-}$*;Ddx4*$^{Cre/+}$ mice.** (**A**) The t-SNE plot of the Cluster1 cells aggregated from the
705 *Foxc2*$^{f/+}$ and *Foxc2*$^{f/-}$*;Ddx4*$^{Cre/+}$ mice colored by sample or subcluster. (**B**) The cell proportion of each
706 sample in each subcluster. (**C**) Feature plots of SPG markers expression. (**D**) Developmental
707 trajectory of the aggregated Cluster1 cells colored by subcluster or pseudotime. (**E**) Expression
708 dynamics of SPG markers with pseudotime progression.
709
710 **Figure 6—source data 1**. Excel spreadsheet with the list of the differentially expressed genes
711 found by scRNA-seq and enriched Gene Ontology terms.
712
713

714 **Figure 7**

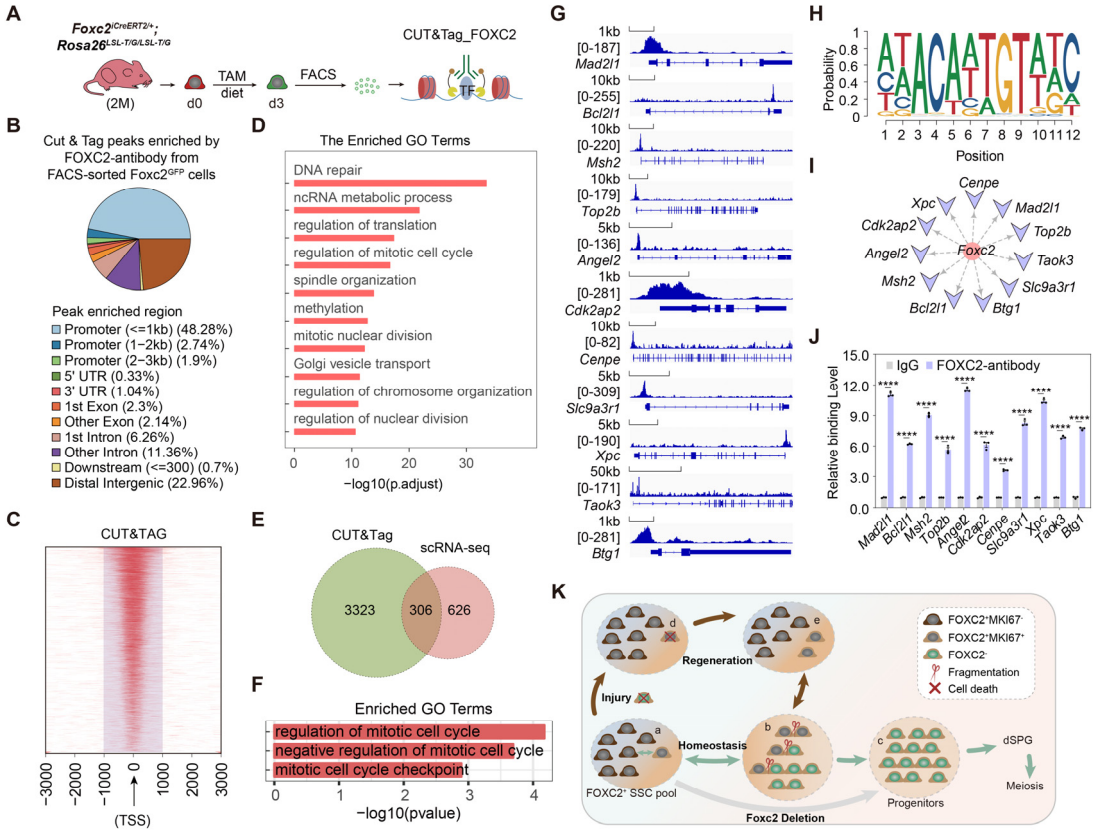

715

716 **FOXC2 is essential for sustaining the quiescent state of SSCs via regulating cell cycle.** (**A**)
717 Workflow schematic illustration of the CUT&Tag_FOXC2 analysis on the FACS-sorted FOXC2$^+$
718 cells. (**B**) Pie chart for CUT&Tag_FOXC2 peaks genome distribution. (**C**) Profiling of
719 CUT&Tag_FOXC2 peaks in proximity to transcriptional starting site (TSS). The distance to TSS
720 within 1000 was highlighted in the purple box. (**D**) Top GO terms enrichment by genes annotated
721 by CUT&Tag_FOXC2 peaks. (**E**) Venn diagram of FOXC2 target genes defined by overlapping the
722 CUT&Tag sequencing and scRNA-seq datasets. (**F**) GO terms enrichment by the FOXC2 target
723 genes related to cell cycle regulation. (**G**) Chromatin landscapes of CUT&Tag_FOXC2 peaks of
724 the candidates associated with negative cell cycle regulation. (**H**) The DNA-binding motif for FOXC2
725 (predicted with HOMER). (**I**) The cell cycle-related candidates possessing high binding potential
726 (>0.8, predicted with JASPAR SCAN). (**J**) CUT&Tag-qPCR validation of the cell cycle arrest
727 regulatory genes. (n=3). Values, mean ± s.e.m.; p-values were obtained using two-tailed t-tests
728 (****p-value < 0.0001). (**K**) The model for the maintenance of the FOXC2$^+$ SSC subpopulation in
729 adult testis.
730

731 **Figure 7—source data 1**. Excel spreadsheet with the list of the differentially expressed genes
732 found by CUT&Tag sequencing and Gene Ontology terms of the 306 crossed candidates.
733

734 **References**

735 Aloisio, G. M., Nakada, Y., Saatcioglu, H. D., Peña, C. G., Baker, M. D., Tarnawa, E. D., Mukherjee,
736 J., Manjunath, H., Bugde, A., Sengupta, A. L., Amatruda, J. F., Cuevas, I., Hamra, F. K., &
737 Castrillon, D. H. (2014). PAX7 expression defines germline stem cells in the adult testis. *J*
738 *Clin Invest*, *124*(9), 3929-3944. https://doi.org/10.1172/jci75943
739 Arai, F., & Suda, T. (2007). Maintenance of quiescent hematopoietic stem cells in the
740 osteoblastic niche. *Ann N Y Acad Sci*, *1106*, 41-53.
741 https://doi.org/10.1196/annals.1392.005
742 Bahar, R., J, O. W., Kawamura, K., Seimiya, M., Wang, Y., Hatano, M., Okada, S., Tokuhisa, T.,
743 Watanabe, T., & Tagawa, M. (2002). Growth retardation, polyploidy, and
744 multinucleation induced by Clast3, a novel cell cycle-regulated protein. *J Biol Chem*,
745 *277*(42), 40012-40019. https://doi.org/10.1074/jbc.M205345200
746 Bahuau, M., Houdayer, C., Tredano, M., Soupre, V., Couderc, R., & Vazquez, M. P. (2002). FOXC2
747 truncating mutation in distichiasis, lymphedema, and cleft palate. *Clin Genet*, *62*(6), 470-
748 473. https://doi.org/10.1034/j.1399-0004.2002.620608.x
749 Bakker, W. J., Blázquez-Domingo, M., Kolbus, A., Besooyen, J., Steinlein, P., Beug, H., Coffer, P. J.,
750 Löwenberg, B., von Lindern, M., & van Dijk, T. B. (2004). FoxO3a regulates erythroid
751 differentiation and induces BTG1, an activator of protein arginine methyl transferase 1. *J*
752 *Cell Biol*, *164*(2), 175-184. https://doi.org/10.1083/jcb.200307056
753 Buaas, F. W., Kirsh, A. L., Sharma, M., McLean, D. J., Morris, J. L., Griswold, M. D., de Rooij, D. G.,
754 & Braun, R. E. (2004). Plzf is required in adult male germ cells for stem cell self-renewal.
755 *Nat Genet*, *36*(6), 647-652. https://doi.org/10.1038/ng1366
756 Cheung, T. H., & Rando, T. A. (2013). Molecular regulation of stem cell quiescence. *Nat Rev Mol*
757 *Cell Biol*, *14*(6), 329-340. https://doi.org/10.1038/nrm3591
758 Clermont, Y. (1966a). Renewal of spermatogonia in man. *Am J Anat*, *118*(2), 509-524.
759 https://doi.org/10.1002/aja.1001180211
760 Clermont, Y. (1966b). Spermatogenesis in man. A study of the spermatogonial population. *Fertil*
761 *Steril*, *17*(6), 705-721.
762 Clermont, Y. (1969). Two classes of spermatogonial stem cells in the monkey (Cercopithecus
763 aethiops). *Am J Anat*, *126*(1), 57-71. https://doi.org/10.1002/aja.1001260106
764 Costoya, J. A., Hobbs, R. M., Barna, M., Cattoretti, G., Manova, K., Sukhwani, M., Orwig, K. E.,
765 Wolgemuth, D. J., & Pandolfi, P. P. (2004). Essential role of Plzf in maintenance of
766 spermatogonial stem cells. *Nat Genet*, *36*(6), 653-659. https://doi.org/10.1038/ng1367
767 Davis, K. E., Moldes, M., & Farmer, S. R. (2004). The forkhead transcription factor FoxC2 inhibits
768 white adipocyte differentiation. *J Biol Chem*, *279*(41), 42453-42461.
769 https://doi.org/10.1074/jbc.M402197200
770 Di Persio, S., Saracino, R., Fera, S., Muciaccia, B., Esposito, V., Boitani, C., Berloco, B. P., Nudo, F.,
771 Spadetta, G., Stefanini, M., de Rooij, D. G., & Vicini, E. (2017). Spermatogonial kinetics in
772 humans. *Development*, *144*(19), 3430-3439. https://doi.org/10.1242/dev.150284
773 Ehmcke, J., & Schlatt, S. (2006). A revised model for spermatogonial expansion in man: lessons
774 from non-human primates. *Reproduction*, *132*(5), 673-680.
775 https://doi.org/10.1530/rep.1.01081
776 Ehmcke, J., Wistuba, J., & Schlatt, S. (2006). Spermatogonial stem cells: questions, models and
777 perspectives. *Hum Reprod Update*, *12*(3), 275-282.
778 https://doi.org/10.1093/humupd/dmk001

Faisal, I., Cisneros-Montalvo, S., Hamer, G., Tuominen, M. M., Laurila, P. P., Tumiati, M., Jauhiainen, M., Kotaja, N., Toppari, J., Mäkelä, J. A., & Kauppi, L. (2019). Transcription Factor USF1 Is Required for Maintenance of Germline Stem Cells in Male Mice. *Endocrinology*, *160*(5), 1119-1136. https://doi.org/10.1210/en.2018-01088

Gallardo, T., Shirley, L., John, G. B., & Castrillon, D. H. (2007). Generation of a germ cell-specific mouse transgenic Cre line, Vasa-Cre. *Genesis*, *45*(6), 413-417. https://doi.org/10.1002/dvg.20310

Gaudet, P., Livstone, M. S., Lewis, S. E., & Thomas, P. D. (2011). Phylogenetic-based propagation of functional annotations within the Gene Ontology consortium. *Brief Bioinform*, *12*(5), 449-462. https://doi.org/10.1093/bib/bbr042

Georgescu, M. M., Cote, G., Agarwal, N. K., & White, C. L., 3rd. (2014). NHERF1/EBP50 controls morphogenesis of 3D colonic glands by stabilizing PTEN and ezrin-radixin-moesin proteins at the apical membrane. *Neoplasia*, *16*(4), 365-374.e361-362. https://doi.org/10.1016/j.neo.2014.04.004

Guo, J., Grow, E. J., Mlcochova, H., Maher, G. J., Lindskog, C., Nie, X., Guo, Y., Takei, Y., Yun, J., Cai, L., Kim, R., Carrell, D. T., Goriely, A., Hotaling, J. M., & Cairns, B. R. (2018). The adult human testis transcriptional cell atlas. *Cell Res*, *28*(12), 1141-1157. https://doi.org/10.1038/s41422-018-0099-2

Guo, R., Yu, Z., Guan, J., Ge, Y., Ma, J., Li, S., Wang, S., Xue, S., & Han, D. (2004). Stage-specific and tissue-specific expression characteristics of differentially expressed genes during mouse spermatogenesis. *Mol Reprod Dev*, *67*(3), 264-272. https://doi.org/10.1002/mrd.20026

Hammoud, S. S., Low, D. H., Yi, C., Carrell, D. T., Guccione, E., & Cairns, B. R. (2014). Chromatin and transcription transitions of mammalian adult germline stem cells and spermatogenesis. *Cell Stem Cell*, *15*(2), 239-253. https://doi.org/10.1016/j.stem.2014.04.006

Hara, K., Nakagawa, T., Enomoto, H., Suzuki, M., Yamamoto, M., Simons, B. D., & Yoshida, S. (2014). Mouse spermatogenic stem cells continually interconvert between equipotent singly isolated and syncytial states. *Cell Stem Cell*, *14*(5), 658-672. https://doi.org/10.1016/j.stem.2014.01.019

Helsel, A. R., Yang, Q. E., Oatley, M. J., Lord, T., Sablitzky, F., & Oatley, J. M. (2017). ID4 levels dictate the stem cell state in mouse spermatogonia. *Development*, *144*(4), 624-634. https://doi.org/10.1242/dev.146928

Hermann, B. P., Cheng, K., Singh, A., Roa-De La Cruz, L., Mutoji, K. N., Chen, I. C., Gildersleeve, H., Lehle, J. D., Mayo, M., Westernströer, B., Law, N. C., Oatley, M. J., Velte, E. K., Niedenberger, B. A., Fritze, D., Silber, S., Geyer, C. B., Oatley, J. M., & McCarrey, J. R. (2018). The Mammalian Spermatogenesis Single-Cell Transcriptome, from Spermatogonial Stem Cells to Spermatids. *Cell Rep*, *25*(6), 1650-1667.e1658. https://doi.org/10.1016/j.celrep.2018.10.026

Jijiwa, M., Kawai, K., Fukihara, J., Nakamura, A., Hasegawa, M., Suzuki, C., Sato, T., Enomoto, A., Asai, N., Murakumo, Y., & Takahashi, M. (2008). GDNF-mediated signaling via RET tyrosine 1062 is essential for maintenance of spermatogonial stem cells. *Genes Cells*, *13*(4), 365-374. https://doi.org/10.1111/j.1365-2443.2008.01171.x

Kanatsu-Shinohara, M., Morimoto, H., & Shinohara, T. (2012). Enrichment of mouse spermatogonial stem cells by melanoma cell adhesion molecule expression. *Biol Reprod*, *87*(6), 139. https://doi.org/10.1095/biolreprod.112.103861

825 Kaya-Okur, H. S., Janssens, D. H., Henikoff, J. G., Ahmad, K., & Henikoff, S. (2020). Efficient low-
826 cost chromatin profiling with CUT&Tag. *Nat Protoc*, *15*(10), 3264-3283.
827 https://doi.org/10.1038/s41596-020-0373-x
828 Kaya-Okur, H. S., Wu, S. J., Codomo, C. A., Pledger, E. S., Bryson, T. D., Henikoff, J. G., Ahmad, K.,
829 & Henikoff, S. (2019). CUT&Tag for efficient epigenomic profiling of small samples and
830 single cells. *Nat Commun*, *10*(1), 1930. https://doi.org/10.1038/s41467-019-09982-5
831 Knudson, C. M., & Korsmeyer, S. J. (1997). Bcl-2 and Bax function independently to regulate cell
832 death. *Nat Genet*, *16*(4), 358-363. https://doi.org/10.1038/ng0897-358
833 Kowalczyk, M. S., Tirosh, I., Heckl, D., Rao, T. N., Dixit, A., Haas, B. J., Schneider, R. K., Wagers, A.
834 J., Ebert, B. L., & Regev, A. (2015). Single-cell RNA-seq reveals changes in cell cycle and
835 differentiation programs upon aging of hematopoietic stem cells. *Genome Res*, *25*(12),
836 1860-1872. https://doi.org/10.1101/gr.192237.115
837 Kubota, H., Avarbock, M. R., & Brinster, R. L. (2004). Culture conditions and single growth factors
838 affect fate determination of mouse spermatogonial stem cells. *Biol Reprod*, *71*(3), 722-
839 731. https://doi.org/10.1095/biolreprod.104.029207
840 Kume, T., Jiang, H., Topczewska, J. M., & Hogan, B. L. (2001). The murine winged helix
841 transcription factors, Foxc1 and Foxc2, are both required for cardiovascular
842 development and somitogenesis. *Genes Dev*, *15*(18), 2470-2482.
843 https://doi.org/10.1101/gad.907301
844 La, H. M., & Hobbs, R. M. (2019). Mechanisms regulating mammalian spermatogenesis and
845 fertility recovery following germ cell depletion. *Cell Mol Life Sci*, *76*(20), 4071-4102.
846 https://doi.org/10.1007/s00018-019-03201-6
847 La, H. M., Mäkelä, J. A., Chan, A. L., Rossello, F. J., Nefzger, C. M., Legrand, J. M. D., De Seram,
848 M., Polo, J. M., & Hobbs, R. M. (2018). Identification of dynamic undifferentiated cell
849 states within the male germline. *Nat Commun*, *9*(1), 2819.
850 https://doi.org/10.1038/s41467-018-04827-z
851 Li, H., Liang, Z., Yang, J., Wang, D., Wang, H., Zhu, M., Geng, B., & Xu, E. Y. (2019). DAZL is a
852 master translational regulator of murine spermatogenesis. *Natl Sci Rev*, *6*(3), 455-468.
853 https://doi.org/10.1093/nsr/nwy163
854 Liao, H. F., Chen, W. S., Chen, Y. H., Kao, T. H., Tseng, Y. T., Lee, C. Y., Chiu, Y. C., Lee, P. L., Lin, Q.
855 J., Ching, Y. H., Hata, K., Cheng, W. T., Tsai, M. H., Sasaki, H., Ho, H. N., Wu, S. C., Huang,
856 Y. H., Yen, P., & Lin, S. P. (2014). DNMT3L promotes quiescence in postnatal
857 spermatogonial progenitor cells. *Development*, *141*(12), 2402-2413.
858 https://doi.org/10.1242/dev.105130
859 Miura, N., Iida, K., Kakinuma, H., Yang, X. L., & Sugiyama, T. (1997). Isolation of the mouse (MFH-
860 1) and human (FKHL 14) mesenchyme fork head-1 genes reveals conservation of their
861 gene and protein structures. *Genomics*, *41*(3), 489-492.
862 https://doi.org/10.1006/geno.1997.4695
863 Motojima, M., Tanimoto, S., Ohtsuka, M., Matsusaka, T., Kume, T., & Abe, K. (2016).
864 Characterization of Kidney and Skeleton Phenotypes of Mice Double Heterozygous for
865 Foxc1 and Foxc2. *Cells Tissues Organs*, *201*(5), 380-389.
866 https://doi.org/10.1159/000445027
867 Nakagawa, T., Jörg, D. J., Watanabe, H., Mizuno, S., Han, S., Ikeda, T., Omatsu, Y., Nishimura, K.,
868 Fujita, M., Takahashi, S., Kondoh, G., Simons, B. D., Yoshida, S., & Nagasawa, T. (2021). A
869 multistate stem cell dynamics maintains homeostasis in mouse spermatogenesis. *Cell
870 Rep*, *37*(3), 109875. https://doi.org/10.1016/j.celrep.2021.109875

871 Nakagawa, T., Nabeshima, Y., & Yoshida, S. (2007). Functional identification of the actual and
872 potential stem cell compartments in mouse spermatogenesis. *Dev Cell*, *12*(2), 195-206.
873 https://doi.org/10.1016/j.devcel.2007.01.002
874 Nakagawa, T., Sharma, M., Nabeshima, Y., Braun, R. E., & Yoshida, S. (2010). Functional
875 hierarchy and reversibility within the murine spermatogenic stem cell compartment.
876 *Science*, *328*(5974), 62-67. https://doi.org/10.1126/science.1182868
877 Nitiss, J. L. (2009). DNA topoisomerase II and its growing repertoire of biological functions. *Nat*
878 *Rev Cancer*, *9*(5), 327-337. https://doi.org/10.1038/nrc2608
879 Oatley, J. M., Avarbock, M. R., & Brinster, R. L. (2007). Glial cell line-derived neurotrophic factor
880 regulation of genes essential for self-renewal of mouse spermatogonial stem cells is
881 dependent on Src family kinase signaling. *J Biol Chem*, *282*(35), 25842-25851.
882 https://doi.org/10.1074/jbc.M703474200
883 Qiu, X., Hill, A., Packer, J., Lin, D., Ma, Y. A., & Trapnell, C. (2017). Single-cell mRNA quantification
884 and differential analysis with Census. *Nat Methods*, *14*(3), 309-315.
885 https://doi.org/10.1038/nmeth.4150
886 Qiu, X., Mao, Q., Tang, Y., Wang, L., Chawla, R., Pliner, H. A., & Trapnell, C. (2017). Reversed
887 graph embedding resolves complex single-cell trajectories. *Nat Methods*, *14*(10), 979-
888 982. https://doi.org/10.1038/nmeth.4402
889 Raman, M., Earnest, S., Zhang, K., Zhao, Y., & Cobb, M. H. (2007). TAO kinases mediate
890 activation of p38 in response to DNA damage. *Embo j*, *26*(8), 2005-2014.
891 https://doi.org/10.1038/sj.emboj.7601668
892 Relaix, F., & Zammit, P. S. (2012). Satellite cells are essential for skeletal muscle regeneration:
893 the cell on the edge returns centre stage. *Development*, *139*(16), 2845-2856.
894 https://doi.org/10.1242/dev.069088
895 Rodgers, J. T., King, K. Y., Brett, J. O., Cromie, M. J., Charville, G. W., Maguire, K. K., Brunson, C.,
896 Mastey, N., Liu, L., Tsai, C. R., Goodell, M. A., & Rando, T. A. (2014). mTORC1 controls
897 the adaptive transition of quiescent stem cells from G0 to G(Alert). *Nature*, *510*(7505),
898 393-396. https://doi.org/10.1038/nature13255
899 Roy, A., Lin, Y. N., Agno, J. E., DeMayo, F. J., & Matzuk, M. M. (2007). Absence of tektin 4 causes
900 asthenozoospermia and subfertility in male mice. *Faseb j*, *21*(4), 1013-1025.
901 https://doi.org/10.1096/fj.06-7035com
902 Sabine, A., Bovay, E., Demir, C. S., Kimura, W., Jaquet, M., Agalarov, Y., Zangger, N., Scallan, J. P.,
903 Graber, W., Gulpinar, E., Kwak, B. R., Mäkinen, T., Martinez-Corral, I., Ortega, S.,
904 Delorenzi, M., Kiefer, F., Davis, M. J., Djonov, V., Miura, N., & Petrova, T. V. (2015).
905 FOXC2 and fluid shear stress stabilize postnatal lymphatic vasculature. *J Clin Invest*,
906 *125*(10), 3861-3877. https://doi.org/10.1172/jci80454
907 Sada, A., Suzuki, A., Suzuki, H., & Saga, Y. (2009). The RNA-binding protein NANOS2 is required
908 to maintain murine spermatogonial stem cells. *Science*, *325*(5946), 1394-1398.
909 https://doi.org/10.1126/science.1172645
910 Sasman, A., Nassano-Miller, C., Shim, K. S., Koo, H. Y., Liu, T., Schultz, K. M., Millay, M., Nanano,
911 A., Kang, M., Suzuki, T., & Kume, T. (2012). Generation of conditional alleles for Foxc1
912 and Foxc2 in mice. *Genesis*, *50*(10), 766-774. https://doi.org/10.1002/dvg.22036
913 Sharma, M., Srivastava, A., Fairfield, H. E., Bergstrom, D., Flynn, W. F., & Braun, R. E. (2019).
914 Identification of EOMES-expressing spermatogonial stem cells and their regulation by
915 PLZF. *Elife*, *8*. https://doi.org/10.7554/eLife.43352

916 Sharma, S., Wistuba, J., Pock, T., Schlatt, S., & Neuhaus, N. (2019). Spermatogonial stem cells:
917 updates from specification to clinical relevance. *Hum Reprod Update*, *25*(3), 275-297.
918 https://doi.org/10.1093/humupd/dmz006
919 Stuart, T., Butler, A., Hoffman, P., Hafemeister, C., Papalexi, E., Mauck, W. M., 3rd, Hao, Y.,
920 Stoeckius, M., Smibert, P., & Satija, R. (2019). Comprehensive Integration of Single-Cell
921 Data. *Cell*, *177*(7), 1888-1902.e1821. https://doi.org/10.1016/j.cell.2019.05.031
922 Suzuki, S., McCarrey, J. R., & Hermann, B. P. (2021). An mTORC1-dependent switch orchestrates
923 the transition between mouse spermatogonial stem cells and clones of progenitor
924 spermatogonia. *Cell Rep*, *34*(7), 108752. https://doi.org/10.1016/j.celrep.2021.108752
925 Tan, K., & Wilkinson, M. F. (2019). Human Spermatogonial Stem Cells Scrutinized under the
926 Single-Cell Magnifying Glass. *Cell Stem Cell*, *24*(2), 201-203.
927 https://doi.org/10.1016/j.stem.2019.01.010
928 Tegelenbosch, R. A., & de Rooij, D. G. (1993). A quantitative study of spermatogonial
929 multiplication and stem cell renewal in the C3H/101 F1 hybrid mouse. *Mutat Res*,
930 *290*(2), 193-200. https://doi.org/10.1016/0027-5107(93)90159-d
931 Tokuda, M., Kadokawa, Y., Kurahashi, H., & Marunouchi, T. (2007). CDH1 is a specific marker for
932 undifferentiated spermatogonia in mouse testes. *Biol Reprod*, *76*(1), 130-141.
933 https://doi.org/10.1095/biolreprod.106.053181
934 Tokue, M., Ikami, K., Mizuno, S., Takagi, C., Miyagi, A., Takada, R., Noda, C., Kitadate, Y., Hara, K.,
935 Mizuguchi, H., Sato, T., Taketo, M. M., Sugiyama, F., Ogawa, T., Kobayashi, S., Ueno, N.,
936 Takahashi, S., Takada, S., & Yoshida, S. (2017). SHISA6 Confers Resistance to
937 Differentiation-Promoting Wnt/β-Catenin Signaling in Mouse Spermatogenic Stem Cells.
938 *Stem Cell Reports*, *8*(3), 561-575. https://doi.org/10.1016/j.stemcr.2017.01.006
939 Toyooka, Y., Tsunekawa, N., Takahashi, Y., Matsui, Y., Satoh, M., & Noce, T. (2000). Expression
940 and intracellular localization of mouse Vasa-homologue protein during germ cell
941 development. *Mech Dev*, *93*(1-2), 139-149. https://doi.org/10.1016/s0925-
942 4773(00)00283-5
943 Trapnell, C., Cacchiarelli, D., Grimsby, J., Pokharel, P., Li, S., Morse, M., Lennon, N. J., Livak, K. J.,
944 Mikkelsen, T. S., & Rinn, J. L. (2014). The dynamics and regulators of cell fate decisions
945 are revealed by pseudotemporal ordering of single cells. *Nat Biotechnol*, *32*(4), 381-386.
946 https://doi.org/10.1038/nbt.2859
947 van Oosten, M., Stout, G. J., Backendorf, C., Rebel, H., de Wind, N., Darroudi, F., van Kranen, H.
948 J., de Gruijl, F. R., & Mullenders, L. H. (2005). Mismatch repair protein Msh2 contributes
949 to UVB-induced cell cycle arrest in epidermal and cultured mouse keratinocytes. *DNA*
950 *Repair (Amst)*, *4*(1), 81-89. https://doi.org/10.1016/j.dnarep.2004.08.008
951 van Velthoven, C. T. J., & Rando, T. A. (2019). Stem Cell Quiescence: Dynamism, Restraint, and
952 Cellular Idling. *Cell Stem Cell*, *24*(2), 213-225.
953 https://doi.org/10.1016/j.stem.2019.01.001
954 Wang, D., Cai, C., Dong, X., Yu, Q. C., Zhang, X. O., Yang, L., & Zeng, Y. A. (2015). Identification of
955 multipotent mammary stem cells by protein C receptor expression. *Nature*, *517*(7532),
956 81-84. https://doi.org/10.1038/nature13851
957 Wang, M., Liu, X., Chang, G., Chen, Y., An, G., Yan, L., Gao, S., Xu, Y., Cui, Y., Dong, J., Chen, Y.,
958 Fan, X., Hu, Y., Song, K., Zhu, X., Gao, Y., Yao, Z., Bian, S., Hou, Y., . . . Qiao, J. (2018).
959 Single-Cell RNA Sequencing Analysis Reveals Sequential Cell Fate Transition during
960 Human Spermatogenesis. *Cell Stem Cell*, *23*(4), 599-614.e594.
961 https://doi.org/10.1016/j.stem.2018.08.007

962 Wang, X., Liu, C., Zhang, S., Yan, H., Zhang, L., Jiang, A., Liu, Y., Feng, Y., Li, D., Guo, Y., Hu, X., Lin,
963 Y., Bu, P., & Li, D. (2021). N(6)-methyladenosine modification of MALAT1 promotes
964 metastasis via reshaping nuclear speckles. *Dev Cell*, *56*(5), 702-715 e708.
965 https://doi.org/10.1016/j.devcel.2021.01.015
966 Weaver, B. A., Bonday, Z. Q., Putkey, F. R., Kops, G. J., Silk, A. D., & Cleveland, D. W. (2003).
967 Centromere-associated protein-E is essential for the mammalian mitotic checkpoint to
968 prevent aneuploidy due to single chromosome loss. *J Cell Biol*, *162*(4), 551-563.
969 https://doi.org/10.1083/jcb.200303167
970 Wei, C., Lin, H., & Cui, S. (2018). The Forkhead Transcription Factor FOXC2 Is Required for
971 Maintaining Murine Spermatogonial Stem Cells. *Stem Cells Dev*, *27*(9), 624-636.
972 https://doi.org/10.1089/scd.2017.0233
973 Yi, X., Hong, M., Gui, B., Chen, Z., Li, L., Xie, G., Liang, J., Wang, X., & Shang, Y. (2012). RNA
974 processing and modification protein, carbon catabolite repression 4 (Ccr4), arrests the
975 cell cycle through p21-dependent and p53-independent pathway. *J Biol Chem*, *287*(25),
976 21045-21057. https://doi.org/10.1074/jbc.M112.355321
977 Yuan, L., Liu, J. G., Zhao, J., Brundell, E., Daneholt, B., & Höög, C. (2000). The murine SCP3 gene is
978 required for synaptonemal complex assembly, chromosome synapsis, and male fertility.
979 *Mol Cell*, *5*(1), 73-83. https://doi.org/10.1016/s1097-2765(00)80404-9
980 Zheng, K., Wu, X., Kaestner, K. H., & Wang, P. J. (2009). The pluripotency factor LIN28 marks
981 undifferentiated spermatogonia in mouse. *BMC Dev Biol*, *9*, 38.
982 https://doi.org/10.1186/1471-213x-9-38

983